The United Nations University

GEOTHERMAL TRAINING PROGRAMME
Orkustofnun, Grensásvegur 9,
IS-108 Reykjavík, Iceland

Reports 2002
Number 10

CORROSION TESTS IN COOLING CIRCUIT WATER AT OLKARIA I PLANT AND SCALE PREDICTIONS FOR OLKARIA AND REYKJANES FLUIDS

Kizito Maloba Opondo
KenGen - Kenya Electricity Generating Company Ltd.
Olkaria Geothermal Project,
P.O.Box 785, Naivasha
KENYA
kopondo@kengen.co.ke

ABSTRACT

Results of corrosion tests conducted on a selection of 6 metallic coupons that had been placed in the cooling water circuit condensates at the Olkaria 1 plant are described with reference to variable pH. The pH of the condensate fluids was adjusted at pH 4, 5, 6, 7 and 9 with the coupons exposed longer at low pH than high pH. Analysis of results obtained by a binocular microscope from the products formed on the coupons are described. Weight changes in the coupons after various exposure periods varying from 2 to 5 days were determined and are presented in the form of plots. Relative chemical composition results for mild steel run in a SEM after exposure at pH 4 in the condensate fluids are presented. A Potential-pH diagram illustrating the stable products that could form from mild steel in the condensate fluids is presented for measured potential and pH. Severe scaling problems have been experienced in Reykjanes wells RN-08 and RN-09, mainly consisting of sulphides and silica deposition. The composition of Reykjanes well fluids was compared to that of Olkaria well fluids from OW-701, OW-706, OW-709 and OW-714 for the prediction of scales that form when fluids boil and cool. Three computer codes, WATCH, SOLVEQ and CHILLER, were used to predict the scales that could form and to determine the saturation temperatures of these fluids with respect to several scale forming minerals. The salinity of Reykjanes wells, which is close to that of sea water, affects the degree of supersaturation and saturation temperatures of the formation of some scales not found in the Olkaria wells. Saturation temperatures for scale formation in the fluids of these wells suggest that silica saturation is reached at higher temperatures in the Reykjanes well fluids than in the Olkaria well fluids. Calcite saturation temperature is lower for the Reykjanes well fluids than the Olkaria well fluids. Calcite remains almost undersaturated in the Olkaria well fluids for OW-701 and OW-706, but well fluids from OW-709 and OW-714 are supersaturated with respect to calcite. The Reykjanes and Olkaria well fluids are undersaturated with respect to anhydrite. Pyrite, which is a sulphide forming scale, is predicted in Olkaria well fluids from OW-709 and OW-714 at temperatures that are lower than those of the Reykjanes well fluids whose sulphide saturation temperatures are very high.

1. INTRODUCTION

In the extraction of heat from fluids in the development of geothermal energy for power production, space heating or process heat, acid or the low pH of fluids can be of significant concern causing corrosion and material problems. In the production of electricity by a direct contact condensing turbine for which cooling circuit water is utilised, acidity of the water is caused by the dissolution of carbon dioxide and hydrogen sulphide gases from the steam. Carbon dioxide dissolves to form weak carbonic acid (H_2CO_3) and hydrogen sulphide is oxidised by oxygen in the cooling circuit water when the water is sprayed into the condenser, to form weak sulphurous acid. In a contact condenser, the steam mixes with the cooling water and condenses and there is no real distinction between cooling water and condensate. The cooling water is circulated back into the cooling tower where further emissions of hydrogen sulphide gas are stripped off by the oxygen-saturated water. This results in the formation of sulphur colloids which coagulate and deposit in the condenser or on the spray nozzles of the cooling tower to form a sulphur scale. The condensate water can become quite acid with the pH affecting the dissolution of the gaseous species. The condensate fluids can be very aggressive to materials that are used in geothermal environments. Typical pH of the condensate water in the Olkaria I power plant is about ~3.0. In this report, pH of both the hot and cold condensate cooling water was adjusted by the use of 3% soda ash dosing, and the aim was to obtain pH 9, 7, 6, 5 and 4. A small pilot project was set up to obtain flows of both cold and hot condensate into holding tanks of ~500 litres. A batch of weighed metal coupons was put in each tank with pH adjusted water and the effects of corrosion studied. The coupons exposed to the condensate fluids were made of materials used in geothermal installations. These included stainless steel 316, stainless steel 304, mild steel, hot dipped galvanized steel, zinc plates, copper, aluminium and brass. Each trial run ranged from 2 to 5 days. Shorter trials were run at the higher pH values of 6 to 9, and longer trials were carried out at the lower pH of 4 and 5. Measurements of potential (Eh), pH, dissolved oxygen (DO) and hydrogen sulphide (H_2S) were carried out regularly on both the undosed and dosed condensate fluids simultaneously. Results of observations by binocular microscope, scanning electron microscope, and on weight changes for a selected number of coupons are presented as well as Potential vs. pH diagrams for iron included in the system Fe-S-H_2O.

During the utilization of geothermal resources for electricity production, large volumes of separated water are disposed of. At each stage, natural hydrothermal fluids that may have been in thermal and chemical equilibrium with heated rocks can be exposed to substantial changes in temperature and pressure, which can affect the solubility of a variety of dissolved mineral species. When the temperature of the fluids decreases the solubility of dissolved silica, metal sulphide species, and some alumin-silicate minerals decreases and they precipitate out of solution either individually or together. Changes in the fluid pressure can lead to a change of state as geothermal fluids ascend to the surface and this can lead to boiling of the liquid and loss of dissolved gases from the geothermal fluid. Boiling of geothermal fluids with a decrease in temperature leads to loss of dissolved gases plus steam and increases the concentration of solids in the residual fluids, enhancing their saturation state. Loss of dissolved gases, especially CO_2 and H_2S from the geothermal fluid, with or without boiling, can also affect the pH of the residual fluid and the solubility of some dissolved minerals, e.g. sulphides, carbonates, silica and some silicates. The boiling and cooling of a geothermal fluid that has a high dissolved solid content often leads to supersaturation with respect to minerals such as calcite and silica which are deposited from solution except in a few cases. These form scales which have a number of detrimental effects like blocking pipelines, blocking production wells which then have to be drilled out, environmental concerns arise, re-injection wells become less permeable due to deposition and drains become blocked. The behaviour of some of the solids deposited in geothermal installations can be significantly affected by small impurities in the brine e.g small concentrations of dissolved Al or Fe causing silica polymerisation and deposition. Other factors like pH, temperature and pressure variations and changes in the silica saturation index affect silica deposition kinetics.

2. CORROSIVE SPECIES IN GEOTHERMAL FLUIDS

2.1 Types of corrosive species

Types of corrosive chemical species encountered in geothermal fluids and their characteristics (Conover et al., 1979) are as follows:

Hydrogen ion. Generally the corrosion rate of carbon steel increases with increasing hydrogen ion concentration (low pH). The increase is more significant below than above pH 7. Likewise the tendency for some alloys to react less in these fluids is also dependent on hydrogen ion concentration. At high pH these alloys form a protective layer or film and corrosion rates are minimised. When the protective layers are broken, this can lead to serious localised attacks which can cause pitting, crevice corrosion, and stress corrosion cracking.

Chloride (Cl^-) causes the local breakdown of the protective films or layers which protect many metals from uniform attack and can lead to pitting, crevice and stress corrosion cracking. Uniform corrosion rates can also increase with increasing chloride concentration.

Hydrogen sulphide (H_2S). The most severe effect is its attack on certain copper and nickel alloys. They are practically unusable in geothermal fluids containing H_2S. The effect of H_2S on iron based materials is less predictable. Increased attack occurs in some cases and inhibition in others. High-strength steels are often subject to sulphide stress cracking. Hydrogen sulphide may cause hydrogen blistering of steels. Oxidation of H_2S in aerated geothermal process streams increases the acidity of the stream.

Carbon dioxide (CO_2). In the acidic region, i.e. as carbonic acid (H_2CO_3), it can accelerate the uniform corrosion of carbon steel. The pH of geothermal fluids and process streams is largely controlled by CO_2. Carbonates and bicarbonates can display mild inhibitive effects.

Ammonia (NH_3) can cause stress corrosion cracking of some copper alloys. It may also accelerate the uniform corrosion of mild steels.

Sulphate (SO_4^{2-}) plays a minor role in most geothermal fluids except in low-chloride fluids in which sulphate is the main aggressive anion.

Oxygen (O_2) concentration of a few ppb or ppm in a high-temperature geothermal fluid can greatly increase the chance of severe localised corrosion of normally resistant metals. Carbon steels are sensitive to trace amounts of oxygen.

Transition metal ions. 'Heavy' or transition metal ions could also be included as key species. Some oxidised forms of transition metal ions (Fe^{3+}, Cu^{2+} and others) are corrosive, but these ions are present in the lowest oxidation state (most-reduced form) in geothermal fluids. Oxygen can convert Fe^{2+} to Fe^{3+}, which is another reason to exclude oxygen from geothermal streams.

2.2 Corrosive modes for metals in geothermal environment

Corrosive attack on metals can occur in several ways and, generally speaking, most modes of corrosion can be found in equipment used in geothermal environments. Conover et al. (1979) discuss some of the main modes of corrosion that occur in geothermal equipment, characterised thus:

Uniform is a major mode of corrosion of low mild steels which attacks the metal surface that is transformed into rust. It is often promoted by chloride, carbon dioxide, oxygen, ammonia or hydrogen ions. This type of corrosion attack can be minimised by applying protective coatings on the surfaces of materials that are prone to it. The rate of uniform corrosion is often very slow in stainless steels.

Pitting corrosion is a localised form of attack and results in the development of small pits on the metal surface. Often it is associated with the breakdown of a protective film or surface scale. Susceptibility to pitting corrosion increases with an increase in chloride and an increase in the hydrogen ion content of the fluid. Electrochemical pitting potential decreases with increasing temperature, which increases the risk of pitting. Stainless steels are most prone to this form of corrosion in high chloride water with pH between 4 and 8.

Crevice corrosion is very similar to pitting corrosion in that it is localised. It depends on the geometry of equipment and forms in crevices of equipment and also under scales deposited. Scales formed on steels by precipitation from geothermal fluids are porous and prone to cracking. Corrosive attack can occur in small exposed areas, particularly if the steel is coupled to a more noble metal.

Stress and sulphide corrosion cracking are types of failure promoted by a combination of factors such as tensile stress, presence of chloride, presence of oxygen and increased temperature which increases the severity of attack. In environments that contain H_2S in aqueous phase, the failure in material is referred to as sulphide stress cracking which could decrease with an increase in temperature, but low pH may greatly accelerate failure.

Other forms of corrosion include *intergranular corrosion, galvanic corrosion, corrosion fatigue, and exfoliation*. Intergranular corrosion is preferential corrosion and involves adjacent boundaries, with little or no attack on the bodies of the grains. Galvanic corrosion occurs when two metals are electrically connected and corrosion of the less noble material will be accelerated. The order of noble material can change with respect to temperature and the chemistry of the environment. Corrosion fatigue results from a premature fracture when cyclic stresses are imposed on a material in a corrosive environment. Exfoliation is the formation of discrete layers of corrosive products or of metal separated from the lattice by corrosive products which break loose and could damage downstream products.

3. DESCRIPTION AND OPERATION OF THE TEST PROCEDURE

Corrosion tests on the condensate fluids of the Olkaria I Power Plant were conducted at variable pH. The pH of the condensate fluids was adjusted by the use of 3% soda ash (sodium carbonate). Condensate holding tanks of approximately 500 litre volume were constructed for the exposure of the metallic coupons from both hot and cold condensate fluids. Condensate was obtained from two locations in the Olkaria I power plant. Cold condensate flows were obtained from the cooling tower basin. This was set up by way of siphoning the condensate at atmospheric pressure to flow into a holding tank. The cold condensate flow from the siphon was adjusted from the side flows in an attempt to achieve a steady flow of ~ 8 kg/min into the holding tank. The temperature of the cold condensate obtained from the cooling tower basin was typically 26˚C. The hot condensate fluid, which is pumped from the seal pit of the condensers was obtained by tapping it from the pipeline that lifts the condensate to the top of the cooling tower. This was directed to a holding tank at an approximately steady flow of ~ 8 kg/min. To facilitate continuous mixing of the condensate in the holding tanks the flow was directed to the bottom and an overflow created at the top so that the contents of the tank were well mixed. Both the cold and hot condensate fluids were fairly aerated although the hot condensate fluids contained relatively less oxygen, because of a relatively high temperature. The holding tanks received condensate that was dosed with 3% sodium carbonate to adjust the pH by varying the rate of injection to 9, 7, 6, 5 and 4 by peristaltic pumping of the sodium carbonate solution. A schematic diagram for the field set-up is shown in Figure 1.

3.1 Condensate chemistry of cooling circuit water.

The chemistry of steam condensates is an important factor in geothermal development particularly with regard to corrosion. This is particularly important when power plant effluent is to be re-injected into re-injection pipelines, wellhead equipment and well casing. Condensate chemistry of cooling water is mostly

controlled by sulphur. The corrosion chemistry of sulphur has been discussed by Lichti et al. (1995), and Bacon et al. (1995). A Potential-pH Pourbaix diagram for the sulphur equilibrium water system indicates that thermo-dynamically the stable dissolved species of sulphur are HSO_4^-, SO_4^{2-}, H_2S, and HS^-. However, by mixing air with hydrogen sulphide, oxidation of hydrogen sulphide does not occur spontaneously and a number of metastable species may form which influence the corrosiveness of the fluid. The presence of hydrogen sulphide in geothermal condensate fluids leads to oxidation with the formation of various sulphur products especially in the open recirculating cooling circuit water due to mixing of condensate with cooling water. The two variables in the condensates of the cooling circuit water that have significant controlling effect on corrosion rates are pH and electrode potential (Eh). The pH is both measurable and controllable. The electrode potential (Eh) is measurable but in the presence of oxygen it can be measured but not controlled. The oxidation of hydrogen sulphide is controlled by the following reaction equations

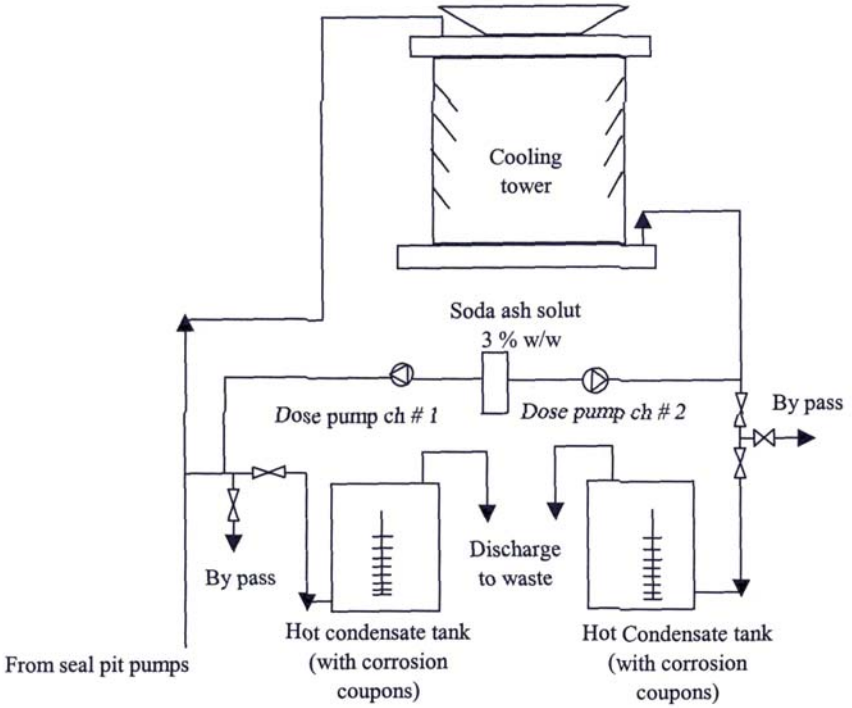

FIGURE 1: Set-up of the field experiment of the corrosion tests with pH adjustment

$$2H_2S + 2O_2 \rightarrow H_2S_2O_3 + H_2O \quad (1)$$

$$5S_2O_3^{2-} + 4O_2 + H_2O \rightarrow 5SO_4^{2-} + H_2SO_4 + S \quad (2)$$

$$4S + 6O_2 + 4H_2O \rightarrow 4H_2SO_4 \quad (3)$$

3.2 Chemistry of the environment for the test

The chemical data available for the corrosion test environment is summarised in Table 1. Some chemical parameters vary considerably between typically undosed hot and cold condensates and dosed condensate fluid. The parameters presented are those thought to influence corrosion. Condensate fluid dosed with 3% sodium carbonate downstream had elevated concentrations of sodium and bicarbonate compared to the undosed condensate.

The hydrogen sulphide gas concentration, which affects pH in the condensates strongly, is high in the hot condensate fluid. The cold condensate fluid was saturated with respect to oxygen and was highly oxidised. The hot condensate had less oxygen and was less oxidised even though it is pumped directly from the condenser seal pit. This is dependent on temperature. Oxygen solubility is reduced as the temperature increases and the temperature of the hot condensate increased slightly. The potential (Eh) measurements made with a platinum electrode suggest that a more reducing environment existed in the hot condensate fluids than in the cold condensates.

TABLE 1: Typical composition of parameters that influence corrosion in condensates, mg/kg

pH	Cl	H_2S	Tot. CO_2	HCO_3	SiO_2	SO_4	NH_3	Fe	DO	Eh (mV)	Temp (˚C)
Typical composition of undosed hot condensate supply											
3.02	16	1.3	Nil	Nil	0.46	94	20	3.5	2.8	-7	45.9
2.95	21	1.4	Nil	Nil	1.00	110	23	4.7	1.9	75	43.2
2.92	22	1.3	Nil	Nil	0.79	86	21	6.5	2.8	27	46.1
Typical composition of dosed hot condensate supply											
8.94	18	1.2	74	74	1.3	112	19	3.5	2.1	-229	46.9
8.06	18	0.68	38	86	0.54	54	18	6.6	0.92	-27	47.6
5.91	23	0.85	28	37	0.67	86	22	6.5	1.0	-155	45
5.3	16	0.61	8.5	7.2	0.54	51	20	7	1.2	-178	45.6
3.78	22	0.51	-	-	2.1	81	21	6.5	1.4	-113	46.1
Typical composition of undosed cold condensate supply											
2.84	18	0.2	Nil	Nil	0.58	67	19.4	6.5	6.8	40	28.4
3.01	15	0.17	Nil	Nil	0.67	86	19.0	5.3	7	434	27.3
3.01	15	0.34	Nil	Nil	1.0	113	18.9	4.8	6.3	438	27.5
Typical composition of dosed cold condensate supply											
9.86	17	-	35	53	2.2	62	16	5.1	5.0	-49	27
6.87	18	0.27	32	38	0.16	59	18	6.3	5.4	128	27
6.0	20	0.24	23	27	0.79	73	19	7.4	5.7	57	26.9
4.76	17	0.17	1	0.98	0.54	75	23	7.5	5.6	244	26.6
4.28	8.5	0.20	0.20	-	0.52	-	21	8.2	6.6	329	26.2

3.3 Experiments

Corrosion tests were conducted using a set of eight metal coupons involving different exposure periods which were dependent on the periods during which the metal coupons were exposed to fluids. The metal coupons were exposed for periods ranging between 2 and 5 days, depending on the duration of the pH test. The pH of condensate fluid was adjusted by injection of 3% sodium carbonate solution. Metal coupons were loaded on a plastic rod, separated by spacers made of the same material. The metal coupons included; hot dipped galvanised steel, mild steel, zinc plates, brass, copper, aluminium, stainless steel 304 and stainless steel 316. The coupons were placed in polyethylene wrappers prior to introducing them into the test environment in the hot and cold condensate tanks in order to eliminate moisture effects. The coupons were weighed to 0.001g accuracy before introducing them into the test environment. Adjusting the test to a new working pH each time, a new set of coupons was introduced into each of the cold and hot condensate holding tanks. Before the start of each new pH adjustment, coupons were removed after the exposure period, air dried and taken to the laboratory. In the laboratory the coupons were stored in a dessicator for about a day and later weighed to 0.001 g. Changes in weight before and after immersion in condensate fluids were used to determine the effects of corrosion for each pH adjustment. Weight loss or gain of each coupon was determined. In this report three mild steel coupons from both the cold and hot condensate fluids at pH 4 and 7 were run in the scanning electron microscope to evaluate products that formed during the pH trials. A ×10 binocular microscope was used to inspect the coupons with. Descriptions of the coupons most affected by the condensate fluids are given in Appendix I.

4. RESULTS

4.1 Binocular microscope inspection

Several methods were used to study results of the products formed upon exposure of the metal coupons to the condensate fluids, such as inspection by a binocular microscope and a scanning electron microscope. Generally, mild steel, copper, brass and galvanised mild steel coupons in the condensate fluids were corroded extensively. Black adherent material and pitting was observed on the mild steel sample, especially that from the hot condensate. From the cold condensate rust-like material, that did not stick very well to the coupon, was observed. Zinc, copper and brass developed dark coatings in both condensates, slight pitting was observed as pH was changed. The stable corrosion products formed on mild steel, zinc plates, copper, brass and galvanised mild steel in the hot condensates were thought to be sulphides of these metals. In the cold condensate which was more aerated and was saturated with respect to oxygen, the main corrosion products appeared to be metallic oxides of the respective metals. For illustration purposes, the stability limits of products of mild steel (iron) have been predicted by the use of Potential-pH Pourbaix diagrams in the system Fe-S-H_2O. The diagrams assist in rationalising the possible corrosion products that could have formed at the measured pH values. The estimated corrosion potential ranges were based on measured results for potential and pH during the tests in the dosed condensate fluids. The Potential-pH diagram for mild steel (iron), (Braithwaite and Lichti, 1979) is here used to predict the stable products formed by iron in the condensate fluids (Figure 2). The Potential-pH (Pourbaix) diagram shows that the corrosion potential for iron at a measured pH of 3.78 and Eh of -178 mV falls in the pyrite stability in the hot condensate, and at measured pH ~ 6 and Eh -155 mV in the haematite field. In the cold condensate at a measured pH 4.28 and ~ 6.87, these fall in the haematite stability field. This supports the observations made under the binocular microscope descriptions for mild steel. Lichti et al. (1998) predicted corrosion potential and pH for a group of alloys in White Island and demonstrated a decrease in corrosion rates on carbon steels by pH adjustment.

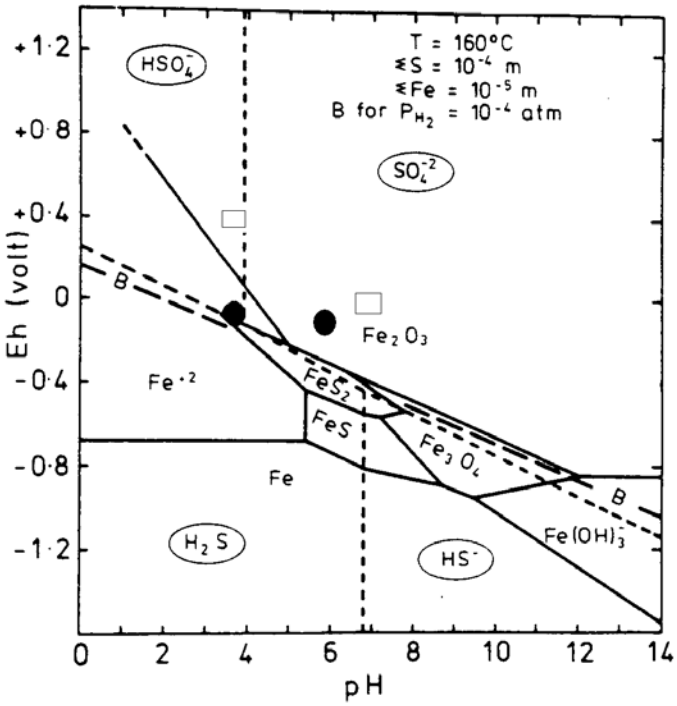

FIGURE 2: Potential-pH diagram for the system Fe-S-H_2O, after Braithwaite and Lichti (1979)
□ Cold condensate fluid ● Hot condensate fluid

4.2 Scanning electron microscope

Three samples of mild steel coupon specimens from the condensate fluids were run in the Scanning Electron Microscope (SEM) at the Technological Institute of Iceland, to illustrate the corrosion products that were formed when the mild steel coupons were exposed to the condensate fluids at pH 4 and 7. In the SEM runs, for the specimens at pH 4 in the cold condensate fluid, the high oxygen and relatively low sulphur concentrations suggest that the main products formed on the mild steel specimens were iron oxides. Trace amounts of aluminium, zinc, or copper are unlikely to have formed from corrosion but most likely result from contamination. The presence of chloride, although in trace amounts, could have led to corrosion producing iron chloride and pitting on the specimen. At pH 4 in the hot condensate fluid, there

was a relatively low level of oxygen on the mild steel specimen compared to that in the cold condensate. Sulphur content is higher in the mild steel specimen exposed to hot condensate fluid than cold one as shown by the SEM runs. Corrosion products on this specimen exposed to hot condensate might consist of iron sulphides with some iron oxides. No trace chloride was detected by the SEM on the specimen from the hot condensate, though pits were evident. One mild steel specimen sample at pH 7 from the cold condensate run in SEM showed a similar trend in component content as the specimen exposed at pH 4. High levels of oxygen and diminished levels of sulphur were observed which could suggest that iron oxides were the dominant corrosion products in this fluid. Trace contents of copper, zinc and aluminium on this specimen suggest contamination. Trace levels of magnesium on this specimen could be derived from cold make-up water from the plant. Iron contents are high in the specimen samples which could result from the base composition of the mild steel. Full results from SEM runs are shown in Appendix II.

4.3 Changes in weight of metal coupons and corrosion rates

Weight changes in the corrosion test coupons are shown in Appendix II and illustrated in Figures 3 and 4 for both the cold and hot condensate at each nominal working pH. Variable rates of corrosion were observed for most metal coupons under test. It is evident from Figures 3 and 4 that metals like zinc, mild steel, brass and copper that were corroded to the greatest extent, lost most weight at pH lower than 5. Corrosion was significant in both cold and hot condensate. In the hot condensate corrosion effects were more evident.

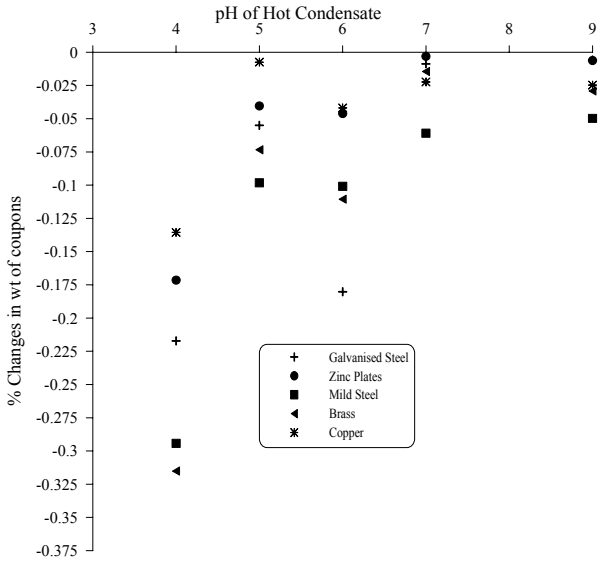

FIGURE 3: Weight changes in metal coupons in hot condensate

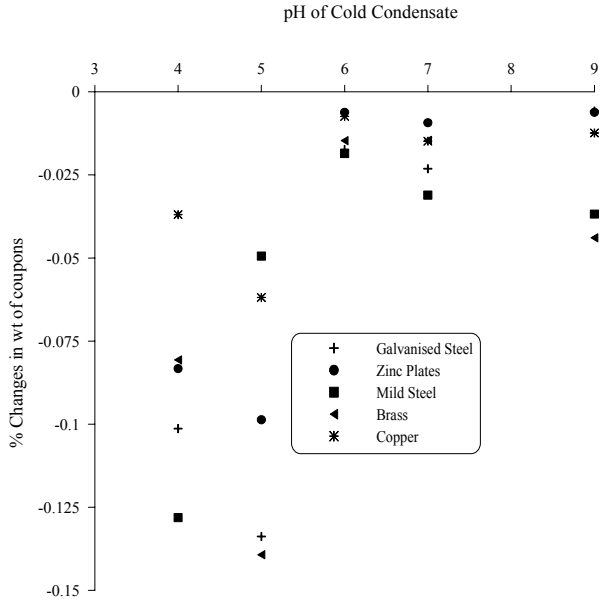

FIGURE 4: Weight changes in metal coupons in cold condensate

The results for the metal specimens that lost significant weight were converted to values of "material loss"and "corrosion rates" using the equations below for each pH adjustment. Material loss was defined as the mean thickness of the material lost by corrosion during an exposure period. Corrosion rates were expressed in the conventional manner as μm/year or converted to mm/yr. The following equations are from Braithwaite and Lichti (1979):

$$ML = (\delta/\rho A) \times 10^3 \quad (4)$$

where ML = Material loss (μm);
δ = Weight loss (mg);
ρ = Test material density (mg/mm^3);

A = Exposed area of test material (mm^2).

$$CR = (ML \times constant) / t \quad (5)$$

where CR = Corrosion rate (μm/year);
ML = Material loss (μm);
$constant$ = 31.557×10^6 (s/mean solar year); and
t = Duration of exposure period (s).

An alternative method, which might be better for estimating corrosion rates, is the calculation of Tafel polarisation curves (see Thórarinsdóttir, 2000) through a graphical method by finding the intersect of the Tafel slope with the projected E_{corr}. This combines the corrosion current (i_{corr}) at the point of intersection and can be used to determine the corrosion rates through the modified Faraday's law equation (Pound et al., 1979):

$$CR = (I_{corr} \times M) / zAF\rho \quad (6)$$

where CR = Corrosion rate (mm/yr);
I_{corr} = Corrosion current (A);
M = Molar mass of metal (g/mole);
A = Area of electrode (mm^2);
z = Number of electrons transferred per metal volume (g/mm^3).

But i_{corr}, the current density, is equal to current applied per unit area of a coupon and the above equation is rewritten as

$$CR = (i_{corr} \times M) / zF\rho \quad (7)$$

Material loss and corrosion rates for each pH adjustment are shown in Table 2 for the metal coupons that showed significant changes in weight.

TABLE 2: Selected coupons material loss and corrosion rate results

		Cold condensate					Hot condensate				
		pH 4	**pH 5**	**pH 6**	**pH 7**	**pH 9**	**pH 4**	**pH 5**	**pH 6**	**pH 7**	**pH 9**
Expo time	(hrs)	120.1	115.25	66	71	45	96	115.25	66	71	45
Galvanised steel	ML	12.08	15.95	2.07	2.76	0.69	25.89	6.556	21.480	1.037	0.696
	CR	879.44	1212.3	274.77	340.60	134.18	2363.80	498.31	2852.93	128.04	135.57
Zinc plates	ML	11.18	13.251	0.83	1.246	0.826	23.03	5.423	6.194	0.413	0.833
	CR	814.12	1007.2	109.7	153.78	106.86	2102.73	412.19	822.68	50.98	162.34
Mild steel	ML	15.03	5.79	2.18	3.64	4.32	34.52	11.83	7.14	5.83	5.83
	CR	1094.0	440.40	289.43	449.78	840.35	3151.92	875.67	1571.18	881.40	1136.53
Brass	ML	15.67	27.06	2.85	2.83	8.53	61.21	14.25	21.48	2.82	5.66
	CR	1141.0	2056.8	378.74	349.37	1662.3	5589.2	1082.9	2852.24	347.98	1102.38
Copper	ML	3.90	6.52	0.78	1.57	1.31	14.29	0.79	4.42	2.36	2.61
	CR	283.56	495.89	103.61	193.27	254.35	1304.66	59.63	586.57	290.85	508.47

ML= Material loss (μm); CR = Corrosion rate (μm/yr)

Corrosion rates were quite variable and at pH 4 and 5 in hot condensate for hot dipped galvanised steel, zinc, brass, mild steel and very high for copper. Similarly corrosion rates were high in cold condensate for metals where corrosion rates were high in hot condensate. Corrosion rates for mild steel varied from 3152 μm/yr at pH 4 to 887 μm/yr at pH 7 in hot condensate. In cold condensate corrosion rates for mild steel varied from 1094 μm/yr at pH 4 to 289 μm/yr at pH 6. At higher pH, mild steel is covered by a

protective layer and corrosion rates are reduced as is evidenced from the results above. The variable corrosion rates, for example at test pH 9, were due to the inability to maintain the pH of the condensate at 9. The pH could drop when the dosing rates were reduced and the condensate pH dropped to near 4. Other potential factors that would affect corrosion rates are dissolved oxygen concentration and the velocity of the condensate fluid. Exposure of the condensate fluids to air lead to oxygen saturation and probable oxidation of hydrogen sulphide gas in cold condensate. Oxygen was present in the hot condensate and this could have led to enhanced corrosion attack on the metal coupons. Under different fluid conditions, simulated steam condensates and much longer exposure periods in low aerated waters like recirculating cooling water, corrosion effects are dependent on temperature, pH, total dissolved sulphur and partial pressure of oxygen (Lichti et al., 1995) . The other metal coupons, copper, brass, and galvanised steel corroded at significant rates at most pH.

The changes in weight loss and corrosion rates may not accurately represent the actual weight loss and corrosion rates due to some steps not being followed in the setting up of the test and in the preparation of the test specimen. Prescribed cleaning procedures for the test specimen were not applied to prepare the test specimens prior to introducing them into the test media and after exposure in the test media themselves. This probably led to overestimation of weight loss changes and in corrosion rates from weight loss. Weight loss techniques measure direct loss of material from a specific surface area after a certain period of exposure. The technique is reliable for measuring an average corrosion rate, but provides no information about momentary changes in corrosion rate, e.g. the response to sudden environmental changes is not obtainable. With electrochemical techniques the momentary corrosion rates can be followed and the effect of different parameters on corrosion rate investigated. Electrochemical techniques, that are applied in corrosion studies are Open Circuit Potential (OCP), Tafel Polarisation, Linear Polarisation Resistance (LPR) and Electrochemical Impedance Spectroscopy (EIS). OCP is a measurement of the corrosion potential, E_{corr}. The value gives important information about the stability of the system, that is if the corrosion products change the corrosion potential of the electrode due to passivity, or if changes in the environment, e.g. varying the oxidising agent, affect the potential in a positive or negative direction. Both LPR and EIS are based on small polarisations and are considered non-destructive to the electrode. They are both widely used for monitoring corrosion rates. The Tafel technique, on the other hand, is a destructive polarisation (Thórarinsdóttir, 2000). Weight loss measurements and corrosion rate calculations are shown in Appendix III. The appropriate corrosion methods that could have been followed for reliable weight loss changes and applied successfully are described in International Standards Organisation (ISO) method Nos. 11845 and 8407. This could have greatly improved the quality of the corrosion tests.

5. SCALING

5.1 General

In the development of geothermal energy, solid scale deposition from geothermal fluids is one the most persistent problems encountered. Scale formation depends on the nature of hydrothermal fluids encountered during geothermal utilization. Geothermal resources vary in character and so do the distribution and content of dissolved solids. Dissolved solids vary considerably from field to field and from around 100 mg/kg in some Icelandic fields, to 250,000 mg/kg in Salton Sea, USA. For most aqueous species, equilibrium between hydrothermal minerals and geothermal reservoir fluid is approached except for a few exceptions e.g chloride and boron (Arnórsson, 1995). These chemicals are dissolved under conditions of elevated temperatures and pressure. During utilization of geothermal resources, the fluid is brought to the surface for the extraction of heat and in the process, this affects the solubility of a variety of dissolved mineral species in several ways. The solubilities of some minerals that are deposited from solution and form scales during utilization are dependent on a variety of factors such as temperature, pressure, pH, the degree of supersaturation, other ions in solution, the degree of aeration and fluid flow

rates. The effect of temperature on the solubility of minerals such as silica, calcite, anhydrite metal sulphides and oxides that are often deposited during production from geothermal resources is reported by miscellaneous workers. For instance the lowering of fluid temperatures can decrease the solubility of dissolved silica or metal sulphide species and allow them to precipitate individually or together.

On the other hand, calcite and a few other minerals like anhydrite become more soluble with decreasing temperatures. They have retrograde solubility and precipitate from solution when temperature increases. Changes in fluid pressure can allow a change of state to take place, either boiling of the fluid or loss of dissolved gases. Boiling decreases both the volume of the residual fluid and concentrates the dissolved solids present, thus increasing their concentration. The loss of dissolved gases, especially soluble gases such as carbon dioxide and hydrogen sulphide from the fluid, also drastically affects the pH of the fluid and the solubility of both sulphides and oxides, silica and carbonate minerals. The solubility of some minerals like silica minerals, metal sulphides and oxides are also dependent on the salinity of the fluids. In low salinity near neutral alkali fluids, silica solubility increases with increased pH. On the contrary, in high salinity and low pH fluids it has been shown that the solubility of silica, metal sulphides and oxides decreases upon change of phase. High magmatic gas concentrations in a reservoir may lead to the formation of sulphide and oxide scales as at Krafla, (Ármarnnsson et al., 1982 and 1989).

In addition to all the above factors in scale formation, in the case of silica the presence of highly charged di- or tri-valent cations like Al^{3+}, Fe^{3+} and Ca^{3+}, in the geothermal fluid would significantly increase the level of colloidal formation and lead to increased deposition rates. In general, the higher the charge on the cation the greater the ability to promote deposition of silica.

5.2 Literature review

A large amount of literature exists on the nature of scale formation, especially silica and carbonates and, to a limited extent, sulphides and oxides and more recently magnesium silicate scales. Most of the effort in the study of scales lays emphasis on the effects of the general parameters discussed above.

Silica and carbonate scales are the ones most extensively studied in connection with geothermal resource utilisation. The precipitated minerals cause problems by restricting fluid flow, preventing valves from closing, scaling turbine blades etc. Chan (1989) reviewed the chemistry of silica deposition. He suggests that it is neither simple nor well understood. Silica deposition depends primarily on fluid kinetics and it can be delayed from minutes to hours after its saturation limit has been exceeded (Rimstidt and Barnes, 1980).

The solubility of silica polymorphs with temperature has been studied extensively. Solubilities of various silica polymorphs with temperature have proven useful as geothermometers (e.g. Arnórsson, 1975; Fournier and Rowe; 1966, Fournier, 1977). Hot water in the reservoir is in equilibrium with quartz and undersaturated with respect to amorphous silica. When a geothermal fluid is brought to the surface, the difference in solubilities between amorphous silica and quartz allows a considerable temperature drop before the solution becomes saturated with respect to amorphous silica. The silica saturation temperature is the temperature at which separated water reaches saturation with respect to amorphous silica. When steam separation takes place above this temperature, then silica scaling usually does not take place and could depend on other dissolved species in the fluid, e.g. Al^{3+} or Fe^{2+} and the fluid salinity. If re-injection is being considered then the temperature is usually kept above the amorphous silica saturation temperature.

The pH dependence of silica solubility is discussed by Henley (1983). He shows that amorphous silica solubility increases markedly as the pH (temperature) is increased. The pH (temperature) as defined by him refers to the pH of the fluid recalculated from analytical data to the temperature of interest, as opposed to that measured directly in the laboratory. In the context of this report, it is the pH after each temperature

decrement with either cooling by steam loss or cooling by conduction without steam loss. Henley (1983) suggests that the higher the gas (CO_2) content of the deep reservoir fluid is, the higher the pH of the residual water. By a careful selection of separation pressures through a two-stage steam extraction system rather than a single-stage one, more gas (CO_2) is extracted into the vapour phase and this in turn raises the pH of the remaining fluid, and may lead to an increase in silica solubility. The pH adjustment in brine clarification plants, with a view to fluid disposal is dependent on brine composition. If brine contains high concentrations of silica or its salinity is high, pH modification is not always successful in preventing silica scale formation (Garcia et al, 1996). At Svartsengi, with brines that are close in salinity to sea water Thórdarson and Tómasson (1989) showed that with pH adjustment an increase in pH and temperatures increased precipitation of silica. Other dissolved salts in geothermal fluid have appreciable effects on silica solubility. At low salinities, there are no marked effects of dissolved species on silica solubility. But as the concentration of other dissolved species, e.g. $NaNO_3$, $MgSO_4$, $MgCl_2$ (Chen and Marshall, 1982), increases in solution the solubility of both quartz and amorphous silica decreases. In highly concentrated solutions the cation influence on amorphous silica solubility decreases in the following order:

$$Mg^{2+} > Ca^{2+} > Sr^{2+} > Li^{+} > Na^{+} > K^{+}$$

Anions also have an effect in the order:

$$I^{-} > Br^{-} > Cl^{-}$$

Pressure effect on silica solubility is generally small compared to temperature (after Fournier and Rowe, 1977; Ragnarsdóttir and Walther, 1983).

Calcite- The other main scaling productin geothermal fluids is calcite and it is a major problem in a number of geothermal areas. Calcium carbonate exists in three different crystalline forms: calcite, aragonite and vaterite. Calcite is thermodynamically most stable, but aragonite is deposited under certain conditions. The formation of calcite in geothermal systems relates to the movement of carbon dioxide through the geothermal system governed by boiling, dilution and condensation. In deep geothermal reservoirs, geothermal fluids are very close to saturation with respect to calcite. Calcite is one of the few minerals that becomes more soluble when temperature of the geothermal fluid is lowered. Ellis (1963) discusses measured solubilities of calcite in solutions containing carbon dioxide. Theoretical aspects of calcite precipitation are discussed by Arnórsson (1989). Important parameters that govern the deposition of calcite include fugacity or partial pressure of carbon dioxide, pH, temperature and the concentration of calcium ions in the geothermal fluid. Increased dissolved CO_2, gas concentration has the effect of increasing calcite solubility with aqueous carbonate species (H_2CO_3, HCO_3^{-}, CO_3^{2-}) mostly controlling the pH. When a geothermal fluid flashes upon boiling as temperature drops with a loss of carbon dioxide gas and in the presence of sufficient amounts of calcium ion concentration, calcite deposition takes place. Field experience (Ármannsson 1989; Benoit 1989) shows that there is a close correspondence between the level of first flashing in the well and the location of the heaviest carbonate deposits in the wells.

Metal sulphide and oxide scales. These occur widely in low-, medium- and high-enthalpy geothermal systems. In high-enthalpy systems with very saline waters such as the Salton Sea California, Asal Djibouti, Milos Greece, Svartsengi and Reykjanes in Iceland sulphide scaling takes place primarily due to the large concentration of metals carried as chloride complexes. Criaud and Foulliac (1989) note that dissolved sulphides of metals such as lead, zinc, copper and iron in geothermal fluids and the utilization schemes and flashing induce deposition of substantial metal sulphide scales. They also note that the conditions of temperature and salinity in a low-temperature environment such as in sedimentary basins, where bacterial action may have occurred, result in high concentrations in the fluids. Líndal (1989) and Hardardóttir et al. (2001) report the formation of different types of sulphide scales at Reykjanes as the operating pressures of the wells are varied. Deposition of these scales was temperature dependent. At Milos Karabelas et al. (1989) observed different composition of scales depending on the location of flashing of fluid. **Other scales** that are found in such environments are iron silicate scales.

Magnesium silicate scaling has been reported in heating systems in Iceland (Kristmannsdóttir et al., 1989) mainly from the mixing of cold deaerated water and geothermal water. Heating of groundwater depletes the magnesium in the water, and magnesium concentration of geothermal water is mostly below 0.1 mg/kg. Anhydrite scale occurrence is widely reported in Philippine geothermal fields (Brown, 1998).

5.3 Chemistry of silica, carbonate, anhydrite and sulphide scale formations

Silica exists in different polymorphic forms, such as quartz, tridymite, cristobalite, amorphous silica, moganite and others. Quartz is the most abundant form of silica in nature. The reservoir rocks of most geothermal systems contain quartz and at the temperatures of the reservoir, quartz dissolves in hot water. Depending on the temperature of the water in the reservoir, equilibrium is established either with chalcedony or quartz. However, the form of silica precipitated at the surface in geothermal water is amorphous but there is growing evidence that it is a finely intergrown mixture of quartz and moganite (Gíslason et al., 1997). Amorphous silica is more soluble than quartz. The solubility of all these silica polymorphs is temperature dependent. Their dissolution in water is represented by the reaction:

$$\underset{\text{Quartz}}{SiO_2\,(s)} + 2H_2O\,(l) \leftrightarrow \underset{\text{Silicic acid}}{H_4SiO_4\,(aq)} \quad (8)$$

The silicic acid dissociates according to the following equation:

$$H_4SiO_4\,(aq) \leftrightarrow H^+ + H_3\,SiO_4^- \quad (9)$$

with

$$K_{eq} = [H^+]\,[H_3SO_4^-] \quad (10)$$

Equilibrium is assumed to exist between the H_4SiO_4 aqueous species and the respective solid phases. The reaction is temperature dependent, approximately following equations put forward by Fournier (1973):

Quartz: $\log C = -1309 / T + 5.19$ (11)

Chalcedony: $\log C = -1032 / T + 4.69$ (12)

Amorphous silica: $\log C = -731 / T + 4.52$ (13)

Amorphous silica deposition proceeds via two types of mechanism, either as molecular or homogenous nucleation. Molecular deposition is effected by silicic acid or silicate ion bound on a growth surface. Homogenous nucleation is effected by condensation reactions to form high molecular weight polymers which then flocculate to form a low density silica scale; this mechanism dominates at high supersaturation. This mechanism proceeds through the combination of silicic acid molecules catalysed by hydroxyl ion with the loss of a water molecule to form dimers, trimers, tetramers etc.

$$H_4SiO_4 + H_4SiO_4 \leftrightarrow H_2O + (HO)_3Si - O - Si(OH)_3 \quad (14)$$

Calcite: Calcium carbonate scales occur in three main polymorphic forms, calcite, aragonite and vaterite. Calcite is thermodynamically most stable but aragonite is deposited under certain circumstances. The solubility of calcite and its deposition from solution is governed by the partial pressure of carbon dioxide, pH, temperature and calcium ion concentration in solution. The solubility of calcite by hydrolysis is described by Arnórrson (1989) according to the reaction

$$CaCO_3 + 2H^+ \leftrightarrow Ca^{2+} + H_2O + CO_2 \quad (15)$$

the equilibrium constant being

$$K_{eq} = pCO_2 \frac{\left[Ca^{2+}\right]}{\left[H^+\right]^2} \tag{16}$$

In geothermal fluid, relatively high concentrations of CO_2 in the presence of a mineral pH buffer will be fixed by the mineral buffers controlling the $[Ca^{2+}]/[H^+]^2$ ratios. Increased dissolved CO_2 concentration (up to about 1 M CO_2) has the effect of increasing calcite solubility with aqueous species (H_2CO_3, HCO_3^-,CO_3^{2-}) mostly controlling pH. Most dissolved CO_2 in geothermal water is present as HCO_3^- or H_2CO_3 and when the fluid has boiled a large part of the CO_2 enters the vapour phase. Calcite deposition with CO_2 loss is described by the chemical reaction:

$$CaCO_3 + CO_2(g) + H_2O \leftrightarrow Ca^{2+} + 2HCO_3^- \tag{17}$$

$$K_{eq} = \frac{\left[Ca^{2+}\right]\left[HCO_3^-\right]^2}{\left[pCO_2\right]} \tag{18}$$

From this reaction dissolved CO_2 is in the form of HCO_3^-, and will be in equilibrium with CO_2 vapour if the gas phase is present. Perturbations may cause CO_2 to be lost from the system and the reaction is driven to the left. This mechanism causes calcite deposition to take place when fluid boils in geothermal environments. The loss of CO_2 gas is dependent on the change in temperature and calcite solubility is also temperature dependent. A parallel reaction is

$$CO_2(aq) + H_2O = H^+ + HCO_3^- \tag{19}$$

Loss of aqueous CO_2 to the gas phase will drive the above reaction to the left, and the pH of the solution will rise. Arnórsson et al. (1982) describes the solubility of calcite with temperature to be governed by the following equation:

$$\log k = 10.22 - 0.0349\,T - \frac{2476}{T} \tag{20}$$

5.4 Mixed sulphide/oxide scales (iron sulphide)

There are many sulphides and oxides that occur in geothermal systems and their solubilities are largely affected by temperature and pressure and change in pH of the fluids. Arnórsson (1995) shows the pH and temperature precipitation dependence of sulphide solids with a specific reference to pyrite**.** He shows that pyrite saturation is dependent on the extent of gas loss in the boiling water, the pH change associated with this boiling, the change in pyrite solubility with temperature and the stability of the Fe^{2+} aqueous in relation to the other Fe-bearing species. The chemical reaction provided for the pyrite solution saturation is

$$FeS_2 + 2H^+ + H_2,aq \leftrightarrow Fe^{2+} + 2H_2S \tag{21}$$

$$K_{eq} = \frac{\left[Fe^{2+}\right]\left[H_2S\right]^2}{\left[H^+\right]^2} \tag{22}$$

The solubility or hydrolysis of pyrite as a function of temperature is given by:

$$\log K_{pyrite} = +565.49 + 0.2000 \times T - 22551 / T - 232.54 \times \log T \tag{23}$$

Other scales that have been reported to form with the mixed oxide scales are iron silicate scales (Gallup, 1989) which are believed to form by reactions of hydrated ferric oxyhydroxide with monosilicic acid or silicic acid oligomers as follows:

$$OFeOH \cdot H_2O + Si(OH)_4 \leftrightarrow Fe(OH)_3 \cdot SiO_2 + 2H_2O \quad (24)$$

Mixed oxide scales such as magnesium silicates show retrograde properties just like calcite. Hauksson and Thórhallsson (1993) concluded, after studies of magnesium silicate scaling with fluids from Nesjavellir and Svartsengi, that the controlling reaction is:

$$MgSiO_3 \cdot H_2O + H_2O \leftrightarrow Mg^{2+} + H_3SiO_4^- + OH^- \quad (25)$$

$$K_{eq} = \left[Mg^{2+} \right] \left[H_3SiO_4^- \right] \left[OH^- \right] \quad (26)$$

with a solubility constant described by

$$\log (ksp) = -12.90 + 0.00262 \times T - 6.212 \times 10^{-5} \times T^2 \quad (27)$$

The formation of the magnesium silicates depends on pH and temperature. Increased temperature and high pH will enhance the rate of precipitation of magnesium silicates. There is an inverse dependence of magnesium silicate solubility with temperature. The major factors that control the degree of supersaturation are boiling temperature and pH.

Anhydrite. Anhydrite scale formation takes place due to the mixing of neutral deep reservoir chloride fluids with shallow acid sulphate water in geothermal systems. The solubility of anhydrite is inversely dependent on temperature. The following reaction describes anhydride dissolution in water:

$$CaSO_4 \leftrightarrow Ca^{2+} + SO_4^{2-} \quad (28)$$

$$K_{eq} = \left[Ca^{2+} \right] \left[SO_4^{2-} \right] \quad (29)$$

The solubility of anhydrite as a function of temperature has been described by Blount and Dickson (1969)

$$\log K_{anhydrite} = +6.20 - 0.0229 \times T - 1217 / T \quad (30)$$

where T = Temperature (K);
$\log K$ = Equilibrium constant.

6. PREDICTING THE FORMATION OF SCALES

Arnórsson (1995) suggests it is possible to predict the conditions at which specific minerals can deposit from water of specified composition during geothermal fluid utilisation. If there is potential for mineral deposition under conditions of e.g. boiling, cooling or heating, it is always desirable to predict the extent to which this can occur. From the chemical composition of produced fluids and with the help of geochemical computer simulation programs such as WATCH (Arnórsson et al., 1982; Bjarnason,1994), SOLVEQ (Reed and Spycher, 2001), CHILLER (Reed and Spycher, 2000), the degree of boiling and mixing processes, the degree of mineral saturation and other reaction processes in aqueous- mineral-gas equilibria are modelled. The programs (computer codes) require an input of the chemical composition of a geothermal fluid from water, steam and condensates. The geochemical computer simulation programs aid in calculating the distribution of activities of aqueous species and mineral saturation indices in natural waters and using hydrothermal reactions from mineral thermodynamic data to evaluate mineral equilibria.

The output from SOLVEQ provides pH species distribution and mineral saturation indices while WATCH provides output for pH, aqueous speciation, partial pressures of gases, redox potentials and activity coefficients and the logarithm of equilibrium constants reaction quotients. The programs can compute the composition of fluids in the deep aquifer from chemical analysis obtained from fluid samples. WATCH has a further capability of recalculating the concentrations of species for conductively cooled fluids or adiabatic boiling from a reference temperature. CHILLER is a sophisticated program for computing complex chemical processes. It can be used for modelling the geochemistry of ore genesis, calculating states of equilibrium in gas-solid-aqueous systems, boiling, cooling, wall rock alteration, groundwater mixing with hot water, acid mixing with metal-bearing fluids and many processes taking place in geothermal systems.

From known chemical composition of well discharges, the state of mineral-solution equilibria can be assessed through thermodynamic considerations. The Gibbs free energy of any chemical reaction, ΔG_r, is given by:

$$\Delta G_r = \Delta G_r^o + RT \ln Q \tag{31}$$

where R = The gas constant;
T = Temperature (K); and
Q = Reaction quotient.

ΔG_r^o, the standard Gibbs free energy of reaction, is given by

$$\Delta G_r^{\,o} = - RT \ln K \tag{32}$$

where K = Equilibrium constant.

The reaction quotient (activity product) for the following general reaction

$$aA + bB = cC + dD \tag{33}$$

is defined as

$$Q = \frac{[\alpha D]^d [\alpha C]^c}{[\alpha B]^b [\alpha A]^a} \tag{34}$$

where α denotes activity.

At equilibrium $\Delta G_r^o = 0$. Thus, from Equations 31 and 32 $K = Q$ at equilibrium. If this reaction is written in such a way that the minimum is on the left hand side, $Q > K$ for oversaturated solution and $Q < K$ for undersaturated solution. The degree of oversaturation / undersaturation is expressed as the ratio Q/K. The log (Q/K) is sometimes referred as the saturation index and symbolised as SI. Aqueous speciation programs such as WATCH, SOLVEQ and CHILLER are used to calculate the activities of individual species from chemical analysis of geothermal fluids, thus obtaining a value for the reaction quotient (Q). Equilibrium constant (K) is obtained from various thermodynamic sources (Arnórsson, 1995).

7. SCALE PREDICTION FOR REYKJANES AND OLKARIA WELL FLUIDS

7.1 Geothermal water chemistry and scale prediction

The chemical composition of fluids from two wells at Reykjanes (Iceland), RN-09 and RN-08, are used to demonstrate the value of chemical thermodynamic assessment of scaling tendencies from geothermal water. The fluid chemistry of these wells is compared to the chemistry of fluids from four selected wells from the Olkaria Northeast geothermal area (Kenya), OW 701, OW-706, OW-709 and OW-714. The chemical composition of these waters differs (Table 3 and 4). The well fluids at Reykjanes are close to seawater salinity while the Olkaria well waters are very dilute. These wells are chosen on the basis of their different fluid characteristics and to demonstrate what kind of scales can be anticipated to deposit at different fluid salinities and processes that affect the fluids as they ascend to the surface upon boiling, conductive cooling and heating. The rates of scale formation depend on the aqueous concentrations of the scale forming components, the degree of the supersaturation and chemical kinetics.

TABLE 3: Chemical composition of water from the two selected Reykjanes and four Olkaria wells (mg/kg) (Orkustofnun and KenGen databases)

	RN-08	**RN-09**	**OW-701**	**OW-706**	**OW-709**	**OW-714**
pH	6.38	5.47	9.48	9.94	9.94	9.61
T for pH (C˚)	20	22.5	20	20	20	20
CO_2	63.1	55.5	126	189	416	186
H_2S	2.21	1.51	5.5	5.7	7	2.7
NH_3	1.7	1.51				
B	8.72	8.63	4.00	4.8	5.6	3.8
SiO_2	631.1	725	779	823	575	803
TDS	39,124	37,220	2,279	2,352	3,340	2,166
Li		4,470	1.87	1.64	1.52	1.2
Na	11,150	10,900	637	536	876	560
K	1,720	1,615	98	99	232	111
Mg	1.44	0.974	0.05	0.04	0.04	0.06
Ca	1,705	1887	0.16	0.07	1.41	0.88
Sr		9.11				
F	0.21	0.20	63	64	58	54
Cl	22,835	21,390	730	544	830	642
SO_4	28.4	16.0	48	25	69	33
Ba		10.0				
Mo		0.0183				
Al	0.07	0.057			0.892	1.053
Cr		0.0014				
Mn		3.81				
Fe	0.329	0.53			0.02	0.02
Cu		0.00081				
Zn		0.0274				
As		0.1				
Ni		0.000144				
Cd		<0.0001				
Sb		0.00334				
Hg		0.0000087				
Pb		0.0014				
Co		0.000390				

TABLE 4: Steam composition of samples from the selected two Reykjanes and four Olkaria wells (mole %)

Well No.	GSP (bar-g)	WHP (bar-g)	Enthalpy (kJ/kg)	CO_2	H_2S	CH_4	H_2	N_2
RN-08	3	19	1150	96.610	2.587	0.155	0.178	0.535
RN-09	4.14	37.5	1310	95.363	4.039	0.009	0.111	0.471
OW-701		4.5	1234	90.867	5.327	0.905	2.313	0.588
OW-706		6.9	1954	96.610	2.587	0.155	0.178	0.535
OW-709	1.9		1955	90.619	2.273	0.254	3.380	3.729
OW-714	2.8		1415	90.208	1.799	0.115	1.330	6.549

GSP = Gas sampling pressure; WHP = Well head pressure.

The geothermal fluid of the above selected wells is assumed to undergo single stage adiabatic boiling with steam loss and conductive cooling as the fluids ascend to the surface from the reservoir. The processes that affect the state of several scale forming minerals is assessed with the assistance of the speciation programs WATCH and CHILLER. Water samples from the Olkaria wells were collected at the well weir box but steam samples at the gas sampling pressures. In the Reykjanes samples, the water and steam were collected at the same sampling pressure (well head pressure). As geothermal fluid boils and cools as it ascends to the surface, it becomes saturated with hydrothermal minerals that are found in the reservoir rocks upon steam loss and loss of dissolved gases. The residual fluid becomes supersaturated with both hydrothermal and scale forming minerals which are deposited from the solution as the fluids cool. Upon the loss of carbon dioxide gas, the pH of the residual liquid increases.

7.2 Fluid saturation state in the six wells

In the assessment of the fluid and the saturation state of the possible troublesome minerals that could be deposited as scales from the fluids of the four wells, WATCH and SOLVEQ were used. CHILLER was used to assess potential of sulphide scale deposits from fluids of well RN-09 at Reykjanes. The chemical data from Tables 3 and 4 above were input in WATCH for a study of the scale forming minerals in the well fluids and the results used to calculate the state of fluid saturation. The output from WATCH details the saturation state for the various minerals after single stage adiabatic boiling with steam loss from an initial reference temperature to a series of preselected temperatures, and after cooling without steam loss from this reference temperature to a series of preselected temperatures. The saturation indices (log Q/K) for anhydrite, chrysotile, calcite, pyrite, amorphous silica, and talc were computed at the chosen temperatures. Measured temperatures were used as reference temperatures for recalculating the chemical composition data to obtain the initial composition of the well fluids except for those of well RN-08 for which the reference temperature was the quartz temperature. Olkaria well temperatures were obtained from Wambugu (1996) but the Reykjanes RN-09 temperature from the Orkustofnun database. Well RN-09 fluid composition was also input in CHILLER and from the output, the formation of sulphide mineral scales of Zn, Pb, Cu, that could be precipitated from solution, was also predicted.

7.3 Anhydrite saturation

The fluids from the 6 wells were analysed for major cations and anions, but fluid from two Olkaria wells had not been analysed for iron and aluminium, important constituents of many hydrothermal minerals and contributors to some of the troublesome scales that are deposited from the residual geothermal fluid, such as magnesium aluminosilicates and iron aluminosilicates. In running WATCH for these samples, iron containing minerals such as pyrite which could be deposited from solution, were not assessed for

supersaturation in Olkaria wells OW-701 and OW-706. The analysis of the samples from the Reykjanes wells and Olkaria wells OW-709 and OW-714, were more complete and included iron and aluminium. Thus, assessment of the saturation state of some iron containing minerals such as pyrite, that could be deposited from solution, was possible. A run was made for well RN-09 using CHILLER to assess possible solid deposition when boiling took place. According to the assessment, chalcopyrite, galena, pyrite and sphalerite are removed from solution between 140 and 100˚C. A run made from CHILLER for RN-09 well fluids is shown in Appendix IV.

Table 5 shows calculated saturation indices, for both single stage adiabatic boiling (with steam loss) and cooling by conduction (no gas loss) for anhydrite saturation for the six wells. The saturation index results are plotted against successive temperature decrements for both adiabatic boiling with steam loss and conductive cooling (Figure 5).

TABLE 5: Anhydrite saturation indices for adiabatic boiling and conductive cooling

Adiabatic boiling (Sat. index) log (Q/K)							**Conductive cooling (Sat. index) log (Q/K)**					
Temp. (˚C)	**RN-08**	**RN-09**	**OW-701**	**OW-706**	**OW-709**	**OW-714**	**RN-08**	**RN-09**	**OW-701**	**OW-706**	**OW-709**	**OW-714**
290				-2.98	-1.84					-2.98	-1.84	
270	0.35		-2.16	-3.10	-1.95	-1.96	0.35		-2.16	-3.33	-1.99	-1.96
250	0.23	0.02	-2.29	-3.25	-2.10	-2.12	0.19	0.02	-2.49	-3.51	-2.15	-2.18
230	0.05	0.06	-2.47	-3.40	-2.26	-2.26	0.001	-0.25	-2.69	-3.70	-2.32	-2.35
210	-0.13	-0.3	-2.67	-3.57	-2.76	-2.42	-0.20	-0.44	-2.89	-3.90	-2.50	-2.54
190	-0.31	0.48	-2.88	-3.73	-2.62	-2.59	-0.40	-0.63	3.10	-4.11	-2.68	-2.72
170	-0.49	-0.66	-3.09	-3.90	-2.81	-2.49	-0.60	-0.82	-3.32	-4.32	-2.87	-2.91
150	-0.67	-0.84	-3.3	-4.07	-2.99	-2.93	-0.79	-1.01	-3.54	-4.54	-3.06	-3.11
130	-0.84	-1.01	-3.51	-4.24	-3.16	-3.12	-0.99	-1.19	-3.76	-4.76	-3.25	-3.31
110	-1.01	-1.17	-3.72	-4.41	-3.51	-3.28	-1.17	-1.38	-3.98	-4.99	-3.45	-3.51
90	-1.16	-1.32	-3.92	-4.58	-3.72	-3.46	-1.35	-1.55	-4.19	-5.21	-3.65	-3.71

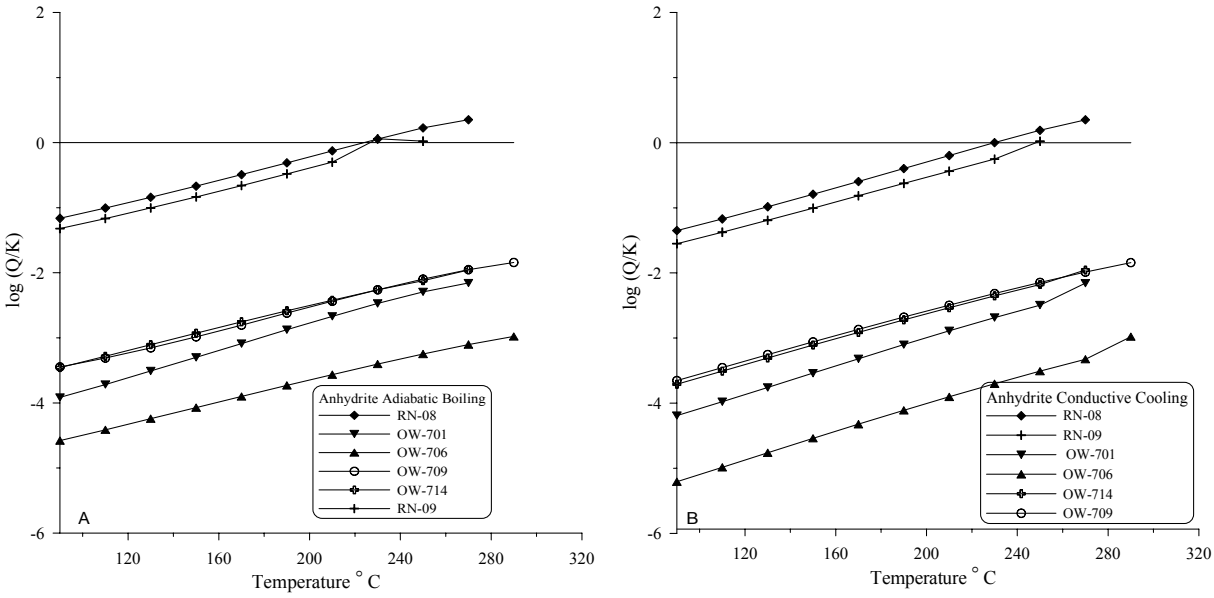

FIGURE 5: Calculated anhydrite saturation state for adiabatic boiling with steam loss and cooling without steam loss, for Olkaria wells OW-701,OW-706,OW-709,OW-714 and Reykjanes wells RN-08 and RN-09

According to predictions from the saturation indices with temperature drop in Olkaria wells' fluids, the fluid is undersaturated with respect to anhydrite at all temperatures. At the highest temperatures just before the onset of boiling and cooling, the saturation indices are higher but as the fluid boils and cools it becomes increasingly undersaturated with respect to anhydrite. The pH of these well fluids is above neutral pH at all temperatures for adiabatic boiling with loss of steam and when the fluids cool without steam loss. This is typical behaviour of anhydrite; as the fluids cool, anhydrite becomes more soluble. From the calculated saturation indices the fluid in the Olkaria wells remains undersaturated with respect to anhydrite at all temperatures and anhydrite is unlikely to precipitate since at the reference temperature the fluid is undersaturated. Anhydrite solubility for fluids from the Reykjanes wells for both adiabatic boiling with steam loss and cooling without steam loss processes, suggest that the deep fluid in both these wells, at temperatures between 225 and 250˚C and above, is either just at saturation or slightly supersaturated with respect to anhydrite. In this temperature range the pH at the temperature of the deep fluid is acid in the range 4.4-5.8. Anhydrite deposition could occur due to low pH of the fluid in the deep water. The chemical composition of fluid in these wells is close to that of sea water and is slightly acid due to high chloride content. Anhydrite supersaturation at this temperature and pH would lead to anhydrite deposition in the reservoir, but as the fluids boil and cool this leads to undersaturation as depicted in Figure 5. At lower temperatures the anhydrite saturation decreases in all cases, although the gradient for the Olkaria well fluids is shifted down compared to the Reykjanes well fluids. These could be attributed to their low salinity. Anhydrite solubility increases when the fluids cool.

7.4 Chrysotile saturation

Table 6 shows calculated saturation indices, for chryostile (a Mg aluminosilicate) saturation for fluids from the six wells. The saturation indices results are plotted against temperature for both adiabatic boiling with steam loss and conductive cooling (Figure 6).

TABLE 6: Chrysotile saturation indices for adiabatic boiling and conductive cooling

Adiabatic boiling (Sat. index) log (Q/K)							**Conductive cooling (Sat. index) log (Q/K)**					
Temp. (˚C)	**RN-08**	**RN-09**	**OW-701**	**OW-706**	**OW-709**	**OW-714**	**RN-08**	**RN-09**	**OW-701**	**OW-706**	**OW-709**	**OW-714**
290				7.40	8.55					7.40	8.55	
270	-2.16		4.79	7.61	8.80	8.30	-2.16		4.79	-1.47	1.69	8.30
250	1.79	-1.61	5.44	7.71	8.98	8.74	-3.48	-1.61	0.04	-3.43	0.02	2.39
230	2.76	-1.49	5.67	7.65	9.06	8.85	-4.95	-9.36	-1.90	-5.46	-1.87	0.53
210	2.99	-1.53	5.70	7.42	9.01	8.77	-6.39	-10.72	-3.83	-7.50	-3.83	-1.43
190	2.87	-1.73	5.60	7.07	8.84	8.52	-7.82	-12.07	-5.72	-9.53	-5.81	-3.41
170	2.53	-2.05	5.43	6.62	8.54	8.15	-9.24	-13.41	-7.57	-11.56	-7.79	-5.39
150	2.05	-2.47	5.23	6.14	8.15	7.71	-10.68	-14.78	-9.39	-13.59	-9.76	-7.37
130	1.49	-2.95	5.00	5.65	7.69	7.23	-12.16	-16.20	-11.20	-15.62	-11.74	-9.35
110	0.89	-3.47	4.76	5.16	7.17	6.73	-13.69	-17.69	-13.00	-17.66	-13.73	-11.35
90	0.28	-4.01	4.50	4.69	6.62	6.23	-15.30	-19.29	-14.83	-19.71	-15.73	-13.36

Predictions of the saturation indices with temperature for the four Olkaria wells show that, with respect to chrysotile, these well fluids are supersaturated when the fluid boils and cools with loss of steam at all temperatures, and that chrysotile will precipitate from solution. The solubility of chrysotile does not seem to depend on pH as the fluid boils and gas loss occurs. As the fluids cool without steam loss, the deep fluid is supersaturated with respect to chrysotile as observed in wells OW-701 and OW-706, at temperatures above 250-270˚C. The saturation temperatures observed, when the fluids cool with steam loss in wells OW-709 and OW-714 in the temperature range 218-245˚C, are slightly lower. The state of supersaturation suggests that chrysotile could be deposited in the reservoir close to measured well temperatures from well fluids of OW-701 and OW-706. As the fluids cool without steam loss to below

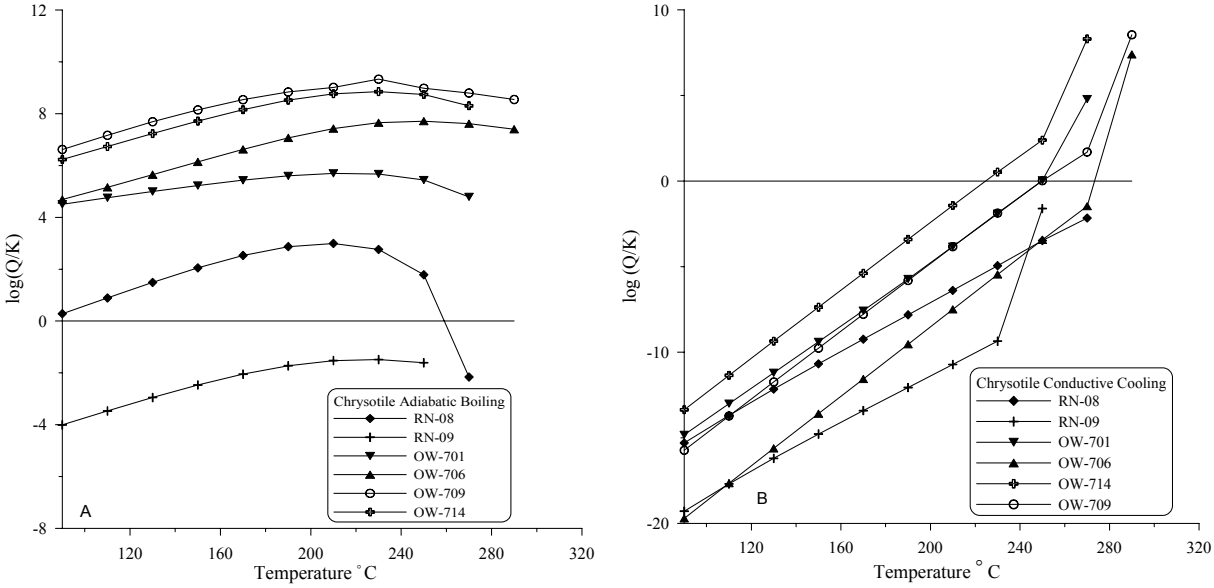

FIGURE 6: Calculated chrysotile saturation state for adiabatic boiling and cooling by conduction, for the four Olkaria and two Reykjanes wells

the saturation temperatures, they become increasingly undersaturated with respect to chrysotile with successive temperature decrements. According to the calculated saturation indices, chrysotile will not be deposited from the residual fluid from the Olkaria wells as the temperatures drop without steam loss.

Chrysotile solubility in the two Reykjanes wells for both boiling with steam loss and cooling without steam loss, suggests that the deep fluid in both wells is undersaturated at almost all well temperatures. Well RN-08, upon adiabatic boiling with steam loss, is undersaturated with respect to chrysotile above ~260˚C. With temperature decrements below ~260˚C on adiabatic boiling, the fluid becomes supersaturate. This suggests that chrysotile supersaturation occurs as temperatures are lowered with steam loss in well RN-08. Depending on the mechanism of temperature decrease that predominates in this well, it is predicted that chrysotile deposition could occur. In well RN-09 the fluid is undersaturated with respect to chrysotile at all the temperatures for both adiabatic boiling and conductive cooling. Chrysotile solubility is expected to increase with decrease in temperatures of the wells.

7.4 Talc saturation

Table 7 shows calculated saturation indices for talc (Mg aluminosilicate) saturation for the six wells. Saturation index results are plotted against successive temperature decreases for both boiling with steam loss and conductive cooling (Figure 7).

Saturation indices with temperature in the four Olkaria wells show for adiabatic boiling that the fluids from these wells are supersaturated with respect to talc at all temperatures. The two Reykjanes wells are also supersaturated with respect to talc for adiabatic boiling. Talc is a hydrothermal magnesium mineral which would probably precipitate from the fluids of these wells due to fluid supersaturation with respect to talc at all the temperatures. The Olkaria well fluids exhibit higher saturation index values for talc than the Reykjanes well fluids. The well fluid of RN-08 is saturated with respect to talc at the bottom temperature. Fluid salinity and high chloride concentration of the Reykjanes well fluids would probably contribute to the lower supersaturation values compared to the Olkaria well fluid composition. Results for cooling without steam loss for the Olkaria well fluids are variable. Well fluids from OW-706, OW-709

TABLE 7: Talc saturation indices for adiabatic boiling and conductive cooling

Adiabatic boiling (Sat. index) log (Q/K)							Conductive cooling (Sat. index) log (Q/K)					
Temp. (˚C)	**RN-08**	**RN-09**	**OW-701**	**OW-706**	**OW-709**	**OW-714**	**RN-08**	**RN-09**	**OW-701**	**OW-706**	**OW-709**	**OW-714**
290				9.27	9.90					9.27	9.90	
270	-0.10		7.07	9.66	10.27	10.26	-0.10		7.07	0.08	2.87	10.26
250	4.20	0.86	7.91	9.94	10.56	10.90	-1.38	0.862	2.44	-1.72	1.36	4.50
230	5.20	1.17	8.34	10.06	10.74	11.16	-2.58	-6.87	0.66	-3.58	-0.37	2.80
210	5.65	1.35	8.56	10.02	10.80	11.24	-3.85	-8.05	-1.09	-5.44	-2.15	1.23
190	5.76	1.39	8.67	9.87	10.74	11.17	-5.08	-9.20	-2.79	-7.28	-3.93	-0.75
170	5.66	1.32	8.73	9.66	10.58	11.01	-6.29	-10.33	-4.41	-9.09	-5.69	-2.51
150	5.46	1.18	8.76	9.43	10.38	10.80	-7.49	-11.46	-5.99	-10.88	-7.42	-4.25
130	5.20	1.01	8.80	9.23	10.15	10.58	-8.69	-12.61	-7.53	-12.63	-9.13	-5.97
110	4.94	0.84	8.71	9.09	9.94	10.4	-9.91	-13.83	-9.02	-14.36	-10.80	-7.65
90	4.73	0.70	8.98	9.01	9.78	10.27	-11.16	-15.03	-10.49	-16.05	-12.45	-9.30

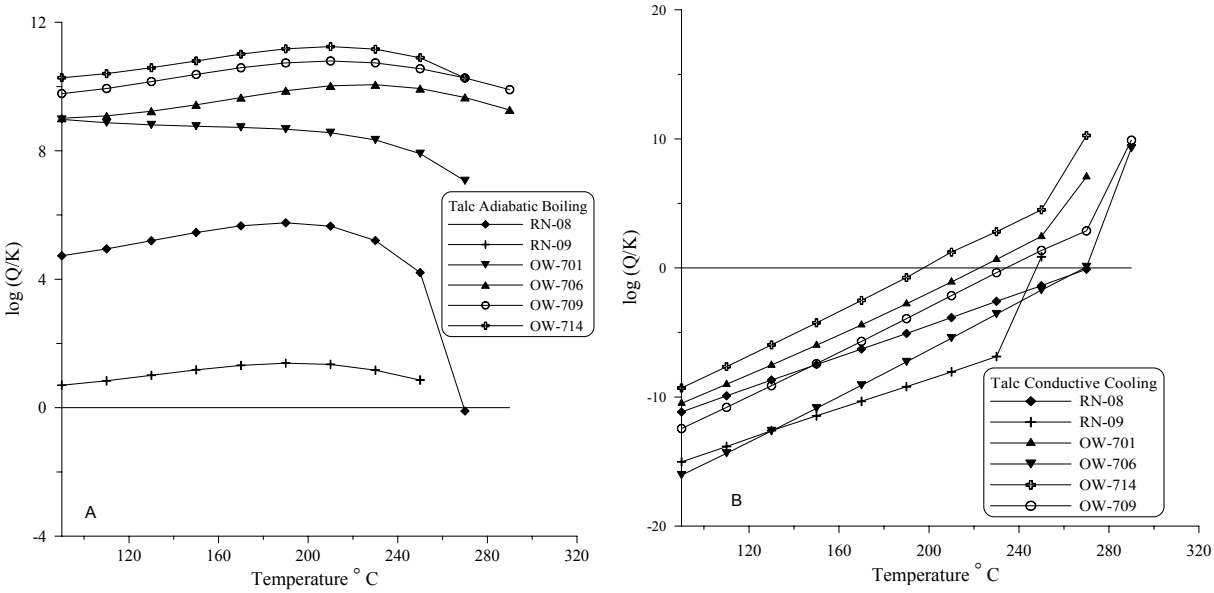

FIGURE 7: Calculated talc saturation state for boiling with adiabatic and conductive cooling, for the six Olkaria and Reykjanes wells

and OW-714, when cooled without steam loss, reach saturation in the temperature range 190-230˚C. As cooling without steam loss is continued, fluids in these wells become undersaturated with respect to talc. Well OW-701 fluids are saturated with respect to talc at higher temperatures. When the fluids are cooled without steam loss, the temperature at saturation is very close to ~270˚C. This temperature is very close to the temperature of the well fluids and suggests that talc saturation temperature is very close to the inflow temperature of the well. Talc deposition is bound to occur above this saturation temperature when the fluids cool without steam loss. Below these temperatures in the Olkaria wells, fluid undersaturation with respect to talc is observed. As the fluids from these wells cool without steam loss, the state of undersaturation suggests that it is unlikely that talc will be deposited. The Reykjanes well fluids exhibit a similar behaviour with respect to cooling without steam loss. Reykjanes well RN-09 fluids are saturated or slightly supersaturated with respect to talc upon cooling without steam loss at very close to the well bottom temperatures. This suggests that talc in this well would precipitate from the residual fluid close to the temperatures of the well above ~ 250˚C. Well RN-08 fluids are just about saturated, with respect to talc, at well temperature but as the fluids cool without steam loss talc undersaturation sets in. The fluids of these wells are bound to remain undersaturated with respect to talc. Upon cooling by steam loss,

no talc deposition would take place at temperatures lower than between 250 and 270˚C. Talc saturation is temperature dependent and as the fluids cool without steam loss, talc becomes undersaturated.

7.5 Pyrite saturation

Table 8 shows calculated saturation indices, for pyrite (sulphide of iron) for fluids from wells RN-08, RN-09, OW-709 and OW-714. Sulphide mineral scale occurrence in the Reykjanes wells has been reported by Hardardóttir et al. (2001). Saturation index results are plotted against successive temperature drop for both boiling with steam loss and cooling without steam loss (Figure 8).

TABLE 8: Pyrite saturation indices for adiabatic boiling and conductive cooling

Adiabatic boiling (Sat. index) log (Q/K)					Conductive cooling (Sat. index) log (Q/K)			
Temp (˚C)	**RN-08**	**RN-09**	**OW-709**	**OW-714**	**RN-08**	**RN-09**	**OW-709**	**OW-714**
290			-82.24				-82.24	
270	-14.90		-70.54	-66.93	-14.90		-38.89	-66.93
250	-14.78	-9.60	-58.86	-54.14	-2.05	-9.60	-22.04	-25.98
230	-8.06	-1.80	-47.20	-43.23	9.47	7.37	-5.35	-9.25
210	0.66	6.18	-35.54	-31.99	14.53	11.15	11.03	7.20
190	9.96	10.74	-23.85	-20.56	18.36	15.08	26.12	22.55
170	17.34	13.60	-12.08	-8.98	22.40	19.29	34.07	31.14
150	21.27	16.41	-0.161	2.72	26.78	23.80	37.47	34.71
130	24.39	19.56	11.95	14.44	31.56	28.69	40.75	38.06
110	27.88	23.22	24.20	25.56	36.82	34.02	44.49	41.85
90	32.02	27.50	35.93	34.59	42.65	39.85	48.94	46.35

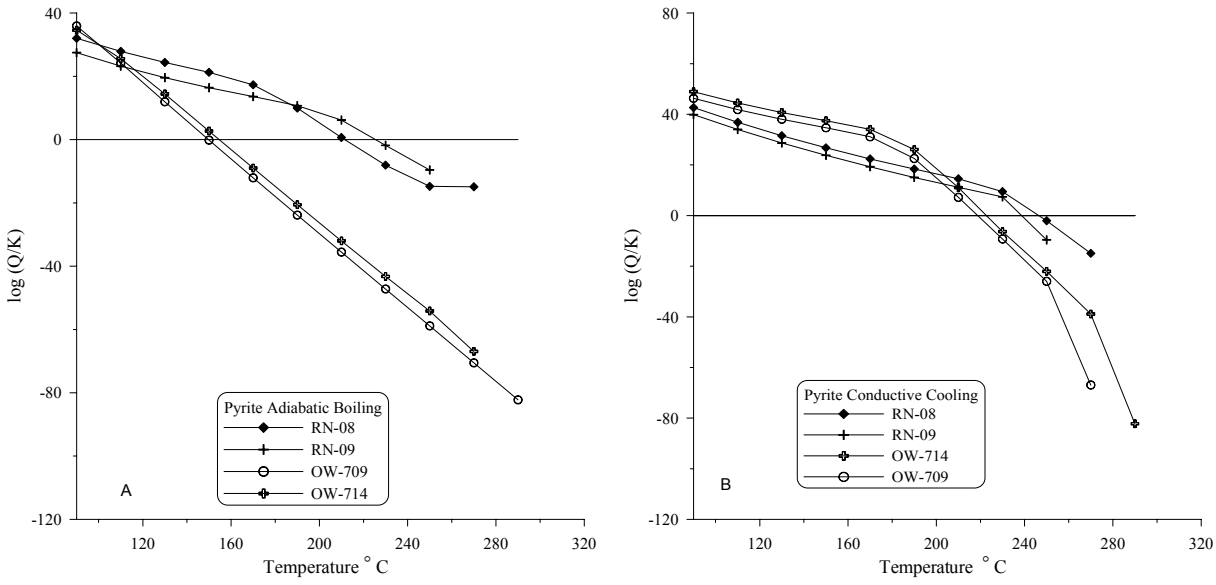

FIGURE 8: Calculated pyrite saturation state for adiabatic boiling and conductive cooling, for the Olkaria wells OW-701, OW-706 and the Reykjanes wells RN-08 and RN-09

The fluids from wells RN-08 and RN-09 are supersaturated with respect to pyrite upon boiling with steam loss in the temperature range 210-230˚C. With continued boiling, pyrite supersaturation is observed. Similarly, when the fluid cools without steam loss it is still supersaturated with respect to pyrite in the residual fluid below 240-250˚C. This suggests that pyrite deposition starts deep in the wells. The pH at

saturation for adiabatic boiling for pyrite in these well fluids is in the range 5.8-6.4. When the fluids cool without loss of steam, the pH for pyrite scale deposition at saturation is about 4.8-5.2. The precipitation of pyrite from the residual fluids of the Reykjanes wells could be pH and temperature dependent. The fluids from the Olkaria wells OW-709 and OW-714 suggest these are saturated with respect to pyrite upon boiling with steam loss in the temperature range of 150-160˚C. With continued boiling and as temperatures decrease, pyrite supersaturation sets in. Below the pyrite saturation temperature, pyrite is likely to precipitate from the residual fluids of these wells. As the fluids from the wells cool without steam loss, the saturation temperatures of pyrite in the well fluids is in the range 220 -225˚C. Below these temperatures the Olkaria well fluids become supersaturated with respect to pyrite when the fluids cool without steam loss and precipitation can take place. If the boiling occurs with steam loss, the pH at the saturation temperatures is in the range 8.75-8.25 but when they cool without steam loss the pH at saturation temperatures is in the range ~ 6.5-6.75. The pH of Olkaria well fluids is higher at temperatures of fluid saturation with respect to pyrite when the fluids cool both by steam loss and without steam loss than that of the Reykjanes well fluids. This could be due to higher carbon dioxide gas content of the Olkaria well fluids.

Karabelas (1986) suggests that when the pH of a geothermal fluid increases due to a temperature reduction as the fluid flashes, the formation of sulphide ions is favoured, leading to the precipitation of most metal sulphides. He further suggests that most metal sulphides are highly insoluble and precipitate rather rapidly from the residual fluid in the presence of suitable metal ions. Criaud and Fouillac (1989) and Honegger et al. (1989) observe that corrosion of mild steel, of which the casing in geothermal wells is composed, can lead to a very large input of iron into the fluid, thus leading to geothermal fluids becoming supersaturated with respect to pyrite early in the upward flow and leading to pyrite deposition. This may not depend on the separation pressures or temperatures of the fluid with respect to pyrite saturation as the corrosion phenomena are not equilibrium processes. The effects of parameters such as pressure, temperature, degassing and addition of iron by corrosion with respect to the saturation indices of pyrite can vary.

7.6 Silica saturation

Table 9 shows calculated saturation indices for both single stage adiabatic boiling and cooling by conduction for silica for fluids from the six wells. Saturation indices are plotted against temperature for both adiabatic boiling with steam loss and cooling by conduction as shown in Figure 9.

TABLE 9: Silica saturation indices for single step adiabatic boiling and conductive cooling

Adiabatic boiling (Sat. index) log (Q/K)							**Conductive cooling (Sat. index) log (Q/K)**					
Temp. (˚C)	**RN-08**	**RN-09**	**OW-701**	**OW-706**	**OW-709**	**OW-714**	**RN-08**	**RN-09**	**OW-701**	**OW-706**	**OW-709**	**OW-714**
290				-0.50	-0.76					-0.50	-0.76	
270	-0.43		-0.32	-0.44	-0.72	-0.47	-0.43		-0.32	-0.68	-0.87	-0.47
250	-0.39	-0.25	-0.25	-0.37	-0.70	-0.41	-0.39	-0.25	-0.29	-0.63	-0.82	-0.43
230	-0.29	-0.19	-0.18	-0.31	-0.68	-0.36	-0.33	-0.27	-0.23	-0.58	-0.76	-0.38
210	-0.21	-0.11	-0.11	-0.25	-0.68	-0.31	-0.27	-0.21	-0.17	-0.51	-0.70	0.31
190	-0.13	-0.02	-0.04	-0.17	-0.63	-0.25	-0.21	-0.15	-0.11	-0.45	-0.64	0.25
170	-0.05	0.07	0.03	-0.10	-0.59	-0.19	-0.14	-0.07	-0.04	-0.38	-0.56	0.18
150	0.05	0.17	0.11	-0.01	-0.54	-0.11	-0.06	0.05	0.04	-0.30	-0.49	0.01
130	0.15	0.27	0.20	0.09	-0.47	-.03	0.03	0.09	0.13	-0.22	-0.40	-0.01
110	0.26	0.39	0.29	0.20	-0.38	0.07	0.12	0.19	0.23	-0.12	-0.30	0.08
90	0.38	0.51	0.39	0.32	-0.26	0.18	0.23	0.29	0.33	0.02	-0.20	-0.19

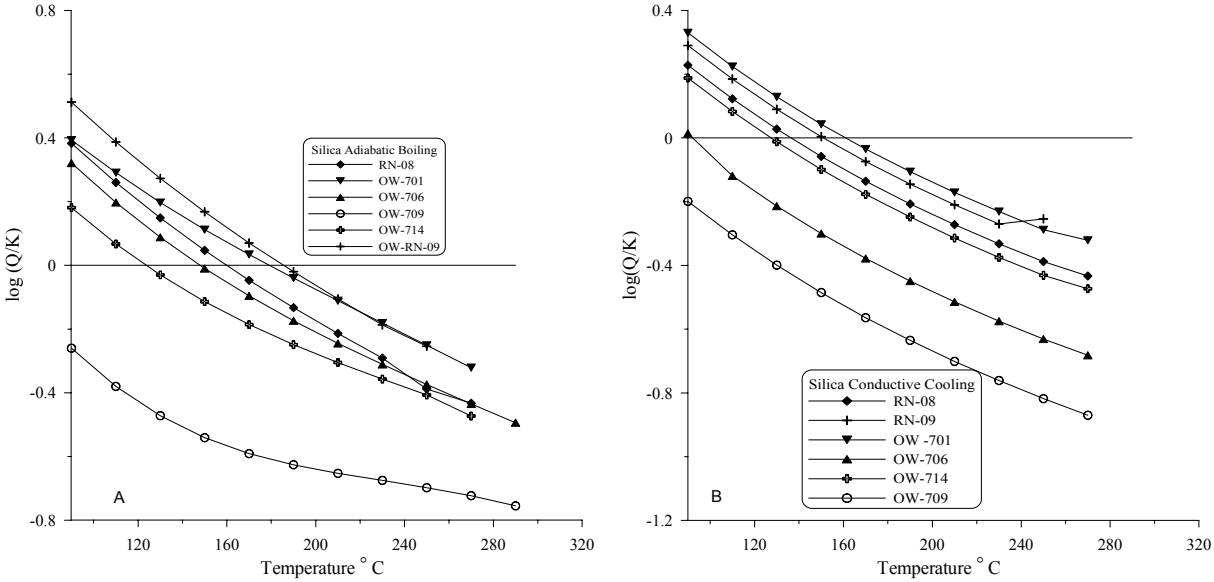

FIGURE 9: Calculated silica saturation state for adiabatic boiling and cooling by conduction, for the six Olkaria and Reykjanes wells fluids

Predictions of the saturation indices with temperature on adiabatic boiling for the Olkaria well fluids are very variable with respect to silica saturation temperature. Well OW-709 fluid is undersaturated with respect to silica at all temperatures. Relatively high silica separation temperatures are observed for fluids of OW-701 and OW-706. For OW-701 fluid the silica separation temperature predicted is ~ 180˚C, and OW-706 fluid ~ 150˚C. Saturation temperature for fluids from OW-714 is lower, or about 120˚C. The pHs of the residual fluids at the respective saturation temperatures are 8.2, 7.75, and 8.75, respectively. The high pH could be the result of the relatively high gas content of the Olkaria fluids. The increased pH in the OW-714 fluid could contribute to the low silica saturation temperature. For OW-709 fluids, the pH at all separation temperatures is the highest and could cause the fluids to be undersaturated with respect to silica. Olkaria well brines are low-salinity brines. The effect of salinity on the activities of water and silicic acid is negligible. The chloride concentrations of the Reykjanes well brines are higher and close to that of sea water. The high salinity of the Reykjanes well brines most likely reduces the solubility of silica compared to that of the Olkaria wells (Henley,1983). For Salton Sea brines, where chloride concentration is approx. 155,000 mg/kg, the solubility of silica at 150˚C is reduced by approximately 60% of its solubility in pure water. The silica separation temperatures for single stage adiabatic boiling observed in the Reykjanes well fluids is higher than that of Olkaria wells. The estimated silica saturation temperature for well RN-08 fluid was ~190˚C and for well RN-09 fluid ~165˚C. The pH_Ts (the pHs at the saturation temperatures) for silica for the two well fluids were ~ 6.6 and 6.0, respectively. Henley (1983) notes that of all factors that affect the silica deposition rate, supersaturation appears to be most significant. The solubility of silica in waste water, resulting from steam separation from geothermal discharges, requires data for the pH_T of the separated water. As noted by Henley (1983), the pH of a geothermal water following steam separation in wellhead separator plants is a function of the composition and temperature and is strongly dependent on the efficiency of gas removal during single stage or multistage steam loss. Applying the silica saturation temperature for single stage adiabatic flash to well fluids of OW-706, and flashing the fluid from 150 to 140˚C, increased the pH slightly but silica supersaturation is still observed.

There is an additional gas loss which occurs during the second stage of adiabatic boiling. Since silica solubility is pH_T dependent, increased silica in the residual fluid would result. For most dilute geothermal fluids, the pH_T values of the residual flashed waters are alkaline (1-2.5 pH units above neutral). In this pH-range, the solubility of silica is strongly dependent on pH_T, as well as on temperature. The pH_T is strongly dependent on the dissolved concentration of carbon dioxide gas in the residual water (Henley,

1983). Silica scale is deposited from the flashed water. Arnórsson (2000) suggests rapid cooling of separated geothermal fluid from high pressure, e.g 6 bar-abs, at Svartsengi to a low-pressure separator of 0.3 bar-abs where, the 160˚C brine flashing to 70˚C quenches amorphous silica deposition, even though the fluid becomes supersaturated with respect to amorphous silica. Deposition does not occur upon re-injection. Gallup (1998) discusses trace amounts of aluminium and iron species which may significantly increase and accelerate precipitation of silica when present in aqueous solutions. Further observation by Gallup (1998) and Thórhallsson et al. (1975) suggests that in the presence of aluminum and iron, iron-rich silicate scales have been observed in Iceland and Salton Sea brines. These tend to be deposited at temperatures as high as between 20 and 75˚C above the silica saturation temperature. A geothermal brine-handling facility, designed to control silica scaling by maintaining brine at conditions of undersaturation to low saturation with respect to pure amorphous silica, may rapidly get clogged by metal silicates in the presence of trace metal ions. Both the Olkaria and Reykjanes well fluids contain trace amounts of aluminum and iron and would require much higher separation temperatures to keep any aluminum- silicates and iron silicates from forming in the residual fluid. At Cerro Prieto I, Milos and Assal, silica deposition can occur very rapidly just at separation or after separation at slight supersaturation as in the presence of trace metal ions. A strong relationship exists between pH and silica solubility. Gudmundsson (1983) showed that at pH≤ 5.5 at Svartsengi silica, polymerisation was not observed in tests conducted in the first 60-80 minutes, but at the original fluid pH of 7.8, polymerisation was rapid.

7.7 Calcite saturation

Table 10 shows calculated saturation indices, for both single stage adiabatic boiling and conductive cooling (no gas loss) for the two Reykjanes and four Olkaria wells. Saturation index results are plotted against temperature for both single step adiabatic boiling with steam loss and conductive cooling. These are shown in Figure 10.

TABLE 10: Calcite saturation indices for single step adiabatic boiling and conductive cooling

Adiabatic boiling (Sat. index) log (Q/K)							**Conductive cooling (Sat. index) log (Q/K)**					
Temp (˚C)	**RN-08**	**RN-09**	**OW-701**	**OW-706**	**OW-709**	**OW-714**	**RN-08**	**RN-09**	**OW-701**	**OW-706**	**OW-709**	**OW-714**
290				0.29	1.88					0.29	2.02	
270	0.25		-0.31	0.15	1.75	1.34	0.25		-0.31	-1.68	0.98	1.34
250	0.81	-0.36	-0.31	0.02	1.63	1.22	0.01	-0.36	-1.16	-2.07	-0.04	0.05
230	0.89	-0.41	-0.37	-0.12	1.51	1.10	-0.25	-1.32	-1.53	-2.46	-0.35	-0.32
210	0.84	-0.49	-0.44	-0.25	1.39	0.98	-0.50	-1.54	-1.90	-2.84	-0.76	-0.68
190	0.73	-0.60	-0.52	-0.38	1.28	0.85	-0.73	-1.76	-2.25	-3.21	-1.11	-1.04
170	0.57	-0.73	-0.60	-0.50	1.18	0.73	-0.96	-1.96	-2.58	-3.58	-1.46	-1.38
150	0.39	-0.88	-0.67	-0.61	1.08	0.61	-1.18	-2.16	-2.91	-3.95	-1.08	-1.73
130	0.21	-1.02	-0.73	-0.71	0.99	0.49	-1.40	-2.35	-3.21	-4.31	-2.13	-2.06
110	0.03	-1.16	-0.77	-0.79	0.91	0.39	-1.61	-2.55	-3.50	-4.67	-2.46	-2.39
90	-0.12	-1.29	-0.79	-0.85	0.85	0.31	-1.82	-2.75	-3.77	-5.00	-2.77	-2.71

Predictions of calcite saturation temperature in the above wells give variable results with no specific trend observed with the variation in salinity of the fluids. Calcite saturation temperature is observed at ~110˚C in the well fluid of RN-08 for adiabatic boiling. Above this temperature calcite supersaturation is observed. Calcite supersaturation in this well increases sharply from the initial temperature of the well to a maximum at ~230˚C before it gradually falls to a saturation temperature of ~110˚C. The pH at the calcite saturation temperature is ~6.3. Below 110˚C, calcite becomes undersaturated and soluble in the residual fluid. The solubility of calcite is predicted to increase with decreasing temperature. When a geothermal fluid boils, boiling is accompanied by loss of carbon dioxide gas. Arnórsson (1995) notes that during the early stages of boiling, loss of gas always predominates causing initially calcite saturated water

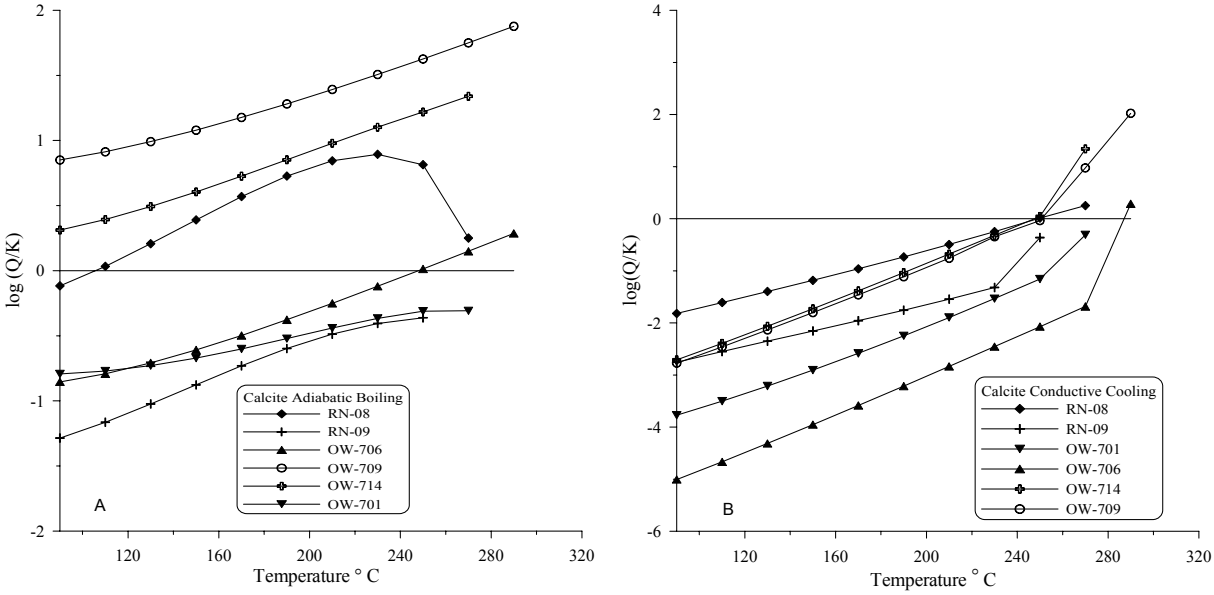

FIGURE 10: Calculated calcite saturation state for adiabatic boiling and cooling by conduction, for the six Olkaria and Reykjanes wells

to become supersaturated. Continued boiling of the geothermal fluid, with loss of gas nearing completion, has the effect of increasing calcite solubility. The residual fluid becomes less supersaturated at lower temperatures and can become undersaturated with respect to calcite. Figure 11 shows the temperature vs. log P_{CO2} partial pressure for the Reykjanes and Olkaria wells with single step adiabatic boiling.

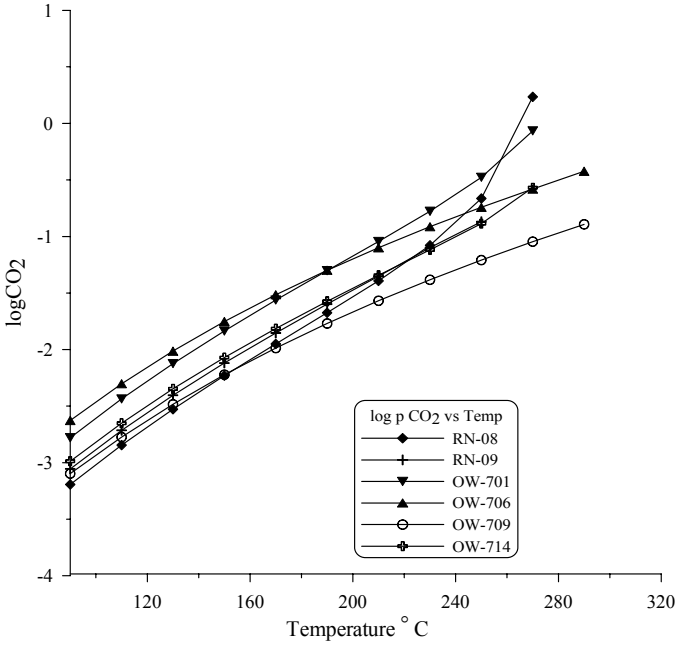

FIGURE 11: Temperature vs. log P_{CO2} in the fluids of the six Reykjanes and Olkaria wells with adiabatic boiling

Fluids of RN-08 are supersaturated with respect to calcite upon adiabatic boiling from inflow temperatures at well bottom to 110˚C. Fluids of Olkaria OW-706 reach calcite saturation temperature at ~250˚C. The pH of this well fluid at calcite saturation temperature is ~7.9. Calcite supersaturation of the fluid declines sharply from the inflow temperature to the saturation temperature of ~250˚C. Below this temperature calcite undersaturation is observed. The calcite saturation temperature for fluids of Olkaria OW-706 is high compared to that of RN-08 fluids The reason for the elevation in the calcite saturation temperature for the Olkaria well fluids upon adiabatic boiling could be high carbon dioxide gas content and the effects of low salinity of the fluid. Arnórsson (1989) suggests that the higher the salinity of the geothermal fluid and the lower its temperature, the higher the degree of calcite supersaturation. Reykjanes RN-09 and Olkaria OW-701 fluids showed no supersaturation with respect to calcite at all the temperatures tested below inflow temperatures. Typically, the degree of undersaturation increased sharply on continued boiling and gas loss. Gas loss upon adiabatic boiling has the effect of increased pH on the residual fluid and this contributes to the level of calcite supersaturation.

Olkaria well OW-709 and OW-714 fluids are supersaturated with respect to calcite at all well temperatures when the fluids cool by steam loss. The pH changes upon gas loss on adiabatic cooling and cooling by conduction with temperature that result from decreased CO_2 gas concentration, are shown in Figure 12.

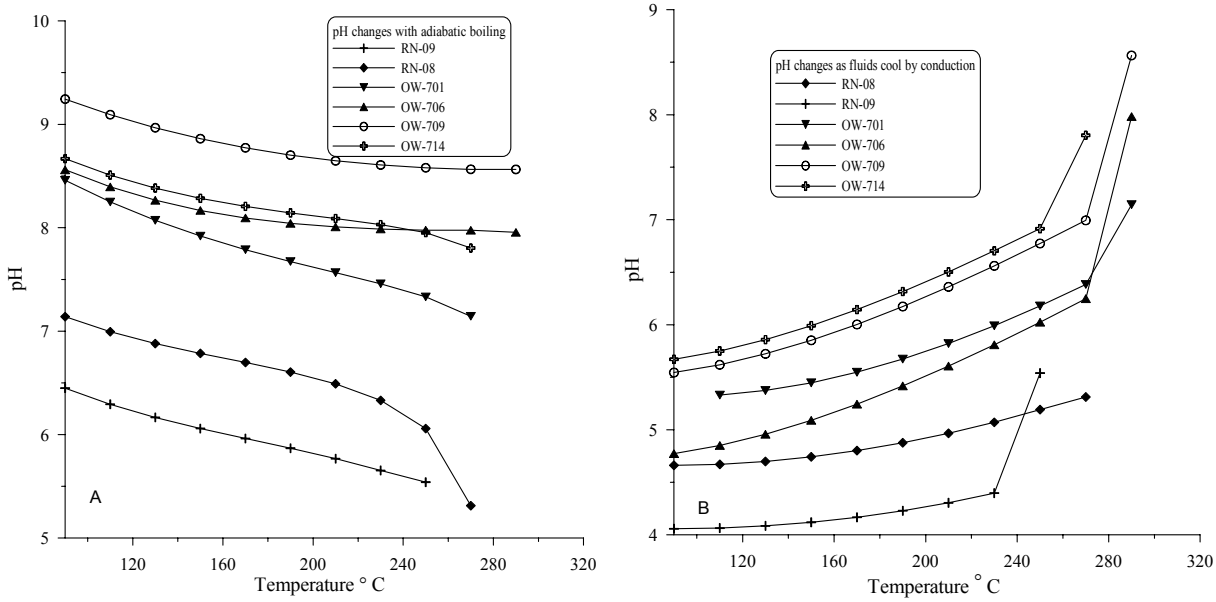

FIGURE 12: pH changes with temperature upon cooling by steam loss and cooling by conduction, for the two Reykjanes and four Olkaria wells

Fluids from OW-701 and RN-09, when cooled by conduction are still undersaturated with respect to calcite. Cooling of fluids by conduction from wells OW-706, OW-709, OW-714 and RN-08 indicates that calcite saturation temperatures are high and very close to the initial temperatures of the wells. Well RN-08 calcite saturation temperature is ~250˚C when the fluids lose heat by conductive cooling. Calcite supersaturation for well RN-08 fluids occurs above ~250˚C. A sharp decline in calcite supersaturation for the inflow temperature of this well drops to 250˚C. Below this temperature, the fluid from RN-08 becomes undersaturated with respect to calcite. For well fluids from OW-706, OW-709, OW-714, calcite saturation temperatures are ~285, ~250 and ~240˚C, respectively, when the fluids cool by conduction. These temperatures are very close to the inflow temperatures of the wells, especially for well OW-706. Calcite saturation occurs at temperatures apparently very close to the measured temperatures of wells OW-706 and RN-08. As the fluid cools conductively, the residual fluids rapidly become undersaturated with respect to calcite. The calcite saturation temperatures of well fluids from OW-709 and OW-714 are slightly lower, or 240-250˚C when the fluids cool by conduction. Above these temperatures, calcite supersaturation is observed. Conductive cooling increases calcite solubility in all these wells. Calcite solubility increases with decrease, in temperature. As the temperatures decrease, undersaturation with respect to calcite sets in. Decreased availability of calcium ions could also contribute to undersaturation. Calcite precipitation often occurs at the first point of flashing upon boiling in the reservoir, but as shown by Ármannsson (1989), it is also dependent upon the flow conditions and the geometry of the wells.

8. CONCLUSIONS

The Olkaria condensate fluids generally corroded coupons of mild steel, copper, brass and galvanised mild steel extensively. Black adherent material and some pitting was observed on the mild steel and zinc plate samples, especially those from the hot condensate. Loose rust-like material that was non-adherent was observed on the mild steel sample from the cold condensate. Dark coatings were observed on zinc, copper

and brass from the hot and cold condensates and slight pitting was observed as the pH of condensate fluids was changed. A potential-pH (Pourbaix) diagram for iron representing mild steel in the system Fe-S-H_2O was used to predict stable iron compounds that formed under the threshold of corrosion. Estimated corrosion potential, based on measured results of potential and pH, showed that the corrosion potential for iron at a measured pH of 3.78 falls in the pyrite stability zone for the hot condensate fluids. In the cold condensate at a measured pH of 4.28 the corrosion potential for iron falls in the haematite stability zone. Significant weight loss for metal coupons of zinc, mild steel, brass and copper were observed at pH lower than 5. Corrosion rates were variable for the metal samples. At pH 4 and 5 in hot condensate corrosion rates for mild steel, copper, brass, hot dipped galvanised steel and zinc were very high. At higher pH of 6-7, the corrosion rates decrease and fall in the haematite stability field. Protective coating on the metal coupons may probably have been formed. SEM results for mild steel at pH 4 suggest higher oxygen content on the specimen exposed to cold condensate than the specimen exposed to hot condensate. Sulphur content on the mild steel specimen was greater in hot than cold condensate fluid.

Mineral scale prediction, based on mineral saturation for fluids of the selected wells OW-701, OW-706, OW-709 and OW-714 at Olkaria and the Reykjanes wells RN-08 and RN-09 reveals different trends and patterns. The Olkaria well fluids are undersaturated with respect to potential scale forming minerals such as anhydrite at all temperatures upon cooling with steam loss. Reykjanes well fluids are saturated or slightly supersaturated with respect to anhydrite at temperatures above 220-250˚C. Below these temperatures the fluids will remain undersaturated with respect to anhydrite. Olkaria well fluids remain supersaturated with respect to chrysotile at all temperatures when the fluids cool accompanied by steam loss. RN-08 fluids are supersaturated with respect to chrysotile to ~240˚C on steam loss, but below it the fluid remains undersaturated with respect to chrysotile. RN-09 fluids remained undersaturated with respect to chrysotile at all temperatures when the fluids were cooled with steam loss. Cooling the well fluids by conduction suggests that they are saturated with respect to chrysotile very close to the inflow well temperatures or altogether undersaturated. When the dominant process is adiabatic cooling, chrysotile deposition will take place in some of the wells. Talc supersaturation is observed at all temperatures in the Olkaria well fluids when they cool with steam loss. Similarly, this trend is observed for the Reykjanes well fluids. When the fluids cool by conduction talc supersaturation is observed above the temperature range 190-230˚C in Olkaria OW-714, OW-709 and OW-706 fluids, while the OW-701 fluid shows higher supersaturation temperatures, above ~270˚C. The RN-09 fluid is just saturated or slightly supersaturated with respect to talc at most well temperatures while the saturation temperatures of RN-08 fluids are very close to the inflow well temperatures when the fluids are cooled by conduction.

Pyrite is a sulphide mineral that can deposit from saline fluids or form because of corrosion. Pyrite saturation temperatures for both cooling with steam loss and without steam loss (conduction) are high in the Reykjanes well fluids. Fluid supersaturation is observed below these temperatures and falls in the temperature range 210-250˚C, with lower pH at pyrite separation temperatures. When the fluids cool by either process below these saturation temperatures, the fluids become supersaturated and pyrite deposition can occur. The Olkaria wells exhibit lower pyrite saturation temperatures, in the range 150-160˚C, with higher pH at pyrite separation temperatures. The saturation state of pyrite or pyrite solubility may also be pH dependent.

Silica solubility depends both on temperature and pH, and the separation temperatures for the Olkaria well fluids are slightly lower than for the Reykjanes well fluids. Silica supersaturation is observed above 150˚C in OW-706 fluid and above 180˚C in OW-701 fluid. Well OW-709 fluid shows undersaturation with respect to silica at all temperatures as fluids cool with steam loss. The pH of the OW-709 fluid is very high and this may also cause undersaturation. The pH at the separation temperature for OW-701 and OW-706 fluids is high and falls to 7.5-8.2, which would increase the solubility of the silica in the residual fluids. Well OW-714 fluid silica saturation temperature is relatively low or ~120˚C with a pH of ~8.75 which could lead to increased silica solubility. The silica separation temperatures are higher and the pH lower at the silica separation temperature in Reykjanes well fluids. These fall within the temperature range 165-190˚C. The pH at these separation temperatures is lower than for the Olkaria wells and falls in the range 6.0-6.6. The solubility of silica decreases at a low pH and possibly also at the relatively high salinities of the Reykjanes well fluids.

The fluids of Olkaria wells OW-709 and OW-714 are supersaturated with respect to calcite at all temperatures when they cool by steam loss. Calcite solubility increases with decrease in temperature and from the results of well RN-08, this suggests a calcite saturation temperature of ~110˚C and a pH of ~6.3. Increase in temperature leads to calcite supersaturation as temperature increases to a maximum of 230˚C in the well fluids. In Olkaria well OW-706 calcite saturation temperature is very high, at ~250˚C and a pH of ~7.9. Calcite solubility is a function of the salinity of a geothermal fluid and dissolved gas in the geothermal fluid. As the salinity of fluid increases, calcite solubility decreases. The salinity of well RN-08 fluid is close to that of sea water. This may be the reason for the decreased solubility of calcite in the well fluids.

ACKNOWLEDGEMENTS

I would like to extend my sincere gratitude to Dr. Ingvar B. Fridleifsson, the Director of the UNU Geothermal Training Programme for offering me a chance to take part in the Programme, and to Deputy Director Lúdvík S. Georgsson, and Gudrún Bjarnadóttir for valuable assistance during my stay at Orkustofnun. I extend my sincere appreciation to my supervisors Dr. Halldór Ármannsson and Vigdís Hardardóttir for valuable guidance and advice during the preparation of this report. To the UNU fellows and the Orkustofnun community, who have been very supportive, many thanks are extended.

I am grateful to the Kenya Electricity Generating Company for granting me sabbatical leave to come and pursue this course. Thanks to my wife Eunice, children Christine Nasike and Esther Narotso for bearing with my absence, and to God Almighty for granting me the strength to endure the course.

Part of the information used in the report is from work done under the supervision of Sinclair Knight and Mertz as part of Contract OG -102 for Olkaria II. Information on Reykjanes was provided by my supervisor, Dr. Halldór Ármannsson.

REFERENCES

Ármannsson, H., 1989: Predicting calcite deposition in Krafla boreholes. *Geothermics, 18*, 25-32.

Ármannsson, H., Benjamínsson, J., and Jeffrey, A.W.A., 1989: Gas changes in the Krafla geothermal system, Iceland. *Chemical Geology, 76,* 175-196.

Ármannsson, H., Gíslason, G., and Hauksson, T., 1982: Magmatic gases in well fluids aid the mapping of the flow pattern in a geothermal system. *Geochim. Cosmochim. Acta, 46,* 167-177.

Arnórsson S., 1975: Application of the silica geothermometer in low-temperature hydrothermal areas in Iceland. *Am. J. Sci., 275*, 763-783.

Arnórsson, S., 1989: Deposition of calcium carbonate from geothermal waters-theoretical considerations. *Geothermics, 18,* 33-89.

Arnórsson, S., 1995: Scaling problems and treatment of separated water before injection. In: Rivera, J. (editor), *Injection technology*. World Geothermal Congress 1995, IGA pre-congress course, Pisa, Italy, May 1995, 65-111.

Arnórsson, S., 2000: Injection of waste geothermal fluids: chemical aspects. *Proceedings of the World Geothermal Congress*, *2000*, *Kyushu-Tohoku, Japan,* 3021-3024.

Arnórsson, S., Sigurdsson, S., and Svavarsson, H., 1982: The chemistry of geothermal waters in Iceland I. Calculation of aqueous speciation from 0˚C to 370˚C. *Geochim. Cosmochim. Acta, 46,* 1513-1532.

Bacon, L., Jordan, J., and Pearson, W., 1995: Microbiology and corrosion in natural draft cooling towers, *Proceedings of the World Geothermal Congress*, *1995, Florence, Italy*, 4, 2387-2389.

Benoit, W., 1989: Carbonate scaling characteristics in Dixie Valley, Nevada geothermal wellbores. *Geothermics, 18*, 41-48.

Bjarnason, J.Ö., 1994: *The speciation program WATCH, version 2.1*. Orkustofnun, Reykjavík, 7 pp.

Blount, C.W., and Dickson, F.W., 1969: The solubility of anhydrite ($CaSO_4$) in NaCl-H_2O from 100 to 450˚C and 1 to 1000 bars. *Geochim. Cosmochim. Acta, 33,* 227-245.

Braithwaite, W.R., and Lichti, K.A, 1979: Surface corrosion of metals in geothermal fluids at Broadlands, New Zealand. In: Casper, L.A., and Pinchback T.R. (eds), *Geothermal scaling and corrosion. ASTM, STP 717*, 32 pp.

Brown, K.L., 1998: *Scaling and geothermal development.* University of Auckland, Geothermal Institute, unpublished lecture notes, 22 pp.

Chan, S.H., 1989: A review on solubility and polymerisation of silica. *Geothermics, 18*, 49-56.

Chen, C.T., and Marshall, W.L., 1982: Amorphous silica solubilities IV. Behaviour in pure water and aqueous sodium chloride, sodium sulphate, magnesium chloride and magnesium sulphate solutions upto 350˚C. *Geochim. Cosmochim. Acta, 46*, 279-287.

Conover, M., Ellis, P., and Curzon, A., 1979: Material selection guidelines for geothermal power systems –An overview. In: Casper, L.A., and Pinchback, T.R., (eds.), *Geothermal scaling and corrosion. ASTM, STP 717*, 17 pp.

Criaud, A., and Fouillac, C., 1989: Sulfide scaling in low-enthalpy geothermal environments: A review. *Geothermics, 18,* 73-81.

Ellis, A.J., 1963: The solubility of calcite in sodium chloride solutions at high temperature. *Amer. J. Sci., 261,* 259-267.

Fournier, R.O., 1973: Silica in thermal waters. Laboratory and field investigations. *Proceedings of the International Symposium on Hydrogeochemistry and Biochemistry, Tokyo, 1, Clark Co., Washington D.C.*, 122-139.

Fournier, R.O., 1977: Chemical geothermometers and mixing models for geothermal systems. *Geothermics, 5*, 41-50.

Fournier, R.O., and Rowe, J.J., 1966: Estimation of underground temperatures from the silica contents of water from hot springs and wet steam wells. *Am. J. Sci., 264,* 685-697.

Fournier, R.O., and Rowe, J.J., 1977: The solubility of amorphous silica in water at high temperatures and high pressures. *Am. Min., 62*, 1052-1056.

Gallup, D.L., 1989: Iron silicate scale formation and inhibition at the Salton Sea geothermal field. *Geothermics, 18*, 97-103.

Gallup, D.L., 1998: Aluminium silicate scale formation and inhibition (2): Scale solubilities and laboratory and field inhibition tests. *Geothermics, 27*, 485-501.

Gíslason, R.S., Heaney, P.J., Oelkers, H.E., and Schott, J., 1997: Kinetic and thermodynamic properties of moganite, a novel silica polymorph. *Geochim. Cosmochim. Acta, 61*, 1193-1204.

Garcia, S.E., Candelaria, M.N.R., Baltazar, A.D.Jr., Solis, R.P., Cabel, A.C.Jr., Nogara, J.B., Reyes, R.L., and Jordan, O.T., 1996: Methods of coping with silica deposition - the PNOC experience. *Proceedings of 17th Annual PNOC-EDC Geothermal Conference, Manila*, 93-109.

Gudmundsson, J.S., 1983: Silica deposition from geothermal brine at Svartsengi, Iceland. *Proc. Symp. Solving Corrosion-Scaling Problems in Geothermal Systems. San Francisco, California,* 72-87.

Hardardóttir, V., Kristmannsdóttir, H., and Ármannsson, H., 2001: Scales formation in wells RN-9 and RN- 8 in the Reykjanes geothermal field Iceland. *Proceedings of the 10th International Symposium* on *Water-Rock Interaction, Villasimius, Italy, Balkema, Rotterdam*, 851-854.

Hauksson, T., and Thórhallsson, S., 1993: *Magnesium silicate deposition. The effect of pH and temperature on the deposition of magnesium silicates from space heating system water (in Icelandic).* Orkustofnun, Reykjavik, report OS-93014/JHD-04, 52 pp.

Honegger, J.L., Czernichowski-Lauriol, I., Criaud, A., Menjoz, A., Sainson, S., and Guenzennec, J., 1989: Detailed study of sulfide scaling at La Courneuve Nord, a geothermal exploitation of the Paris Basin, France. *Geothermics, 18*, 137-144.

Henley, R.W., 1983: pH and silica scaling control in geothermal field development. *Geothermics, 12*, 307-321.

Karabelas, A.J., 1986: Factors influencing scale formation in geothermal installation. In: *Corrosion et entartrage dans les systèmes géothermaux.*. Contractors meeting on corrosion and scaling, Commission of the European Communities, B.R.G.M, 11 pp.

Karabelas, A.J., Andritsos, N., Mouza, A., Mitrakas, M., Vrouzi, F., and Christanis, K., 1989: Characteristics of scales from the Milos geothermal plant. *Geothermics, 18*, 169-174.

Kristmannsdóttir, H., Ólafsson, M., and Thórhallsson, S., 1989: Magnesium silicate scaling in district heating systems in Iceland. *Geothermics, 18*, 191-198.

Lichti K.A., Graham, V.J., Engelberg, D., Sanada, N., Kurata, Y., Nanjo, H., Ikeuchi, J., and Christenson, B.W., 1998: Corrosion properties of volcanic hot springs. *Proceedings of the 20th New Zealand Geothermal Workshop, Geothermal Institute, Auckland,* 97-102.

Lichti K.A., Johnson, C.A., McIlhone, P.G.H., and Wilson, P.T., 1995: Corrosion of iron-nickel base and titanium alloys in aerated geothermal fluids. *Proceedings of the World Geothermal Congress 1995*, Florence, Italy, 4, 2375-2380.

Líndal, B., 1989: Solids deposition in view of geothermal applications in Reykjanes and Svartsengi, south western Iceland. *Geothermics, 18*, 207-216.

Pound, B.G., Abdurrahman, M.P., Glucina, M.P., Sharp, R.M., and Wright, G.A., 1979: The measurement of corrosion rates of carbon steel in geothermal media by the polarisation resistance technique. *Proceedings of the 2nd New Zealand Geothermal Workshop*, *Geothermal Institute, University of Auckland, NZ,* 97-100.

Ragnarsdóttir, K.V., and Walther, J.W., 1983: Pressure sensitive 'silica geothermometer' determined from quartz solubility experiments at 250˚C. *Geochim. Cosmochim. Acta, 47*, 941-946.

Reed, M.H., and Spycher, N., 2000: *User´s guide for CHILLER: A program for computing- liquid-rock reactions, boiling, mixing and other reaction processes in aqueous-mineral-gas systems* (revised ed.). Department of Geological Sciences, University of Oregon, Eugene, OR, 67 pp.

Reed, M.H., and Spycher, N., 2001: *User´s guide for SOLVEQ: a computer program for computing aqueous-minerals- gas equilibria* (revised ed.). Department of Geological Sciences, University of Oregon, Eugene, OR, 38 pp.

Rimstidt, J.D., and Barnes, H.L., 1980: The kinetics of silica-water reactions. *Geochim. Cosmochim. Acta, 44*, 1683-1699.

Thórdarson, H., and Tómasson, Th.H., 1989: Brine clarification at Svartsengi, Iceland: effect of pH and temperature on the precipitation of silica and its properties. *Geothermics, 18*, 287-294.

Thórhallsson, S., Ragnars, K., Arnórsson, S., and Kristmannsdóttir, H., 1975: Rapid scaling of silica in two district heating systems. *2nd United Nations Symposium on the Development and Use of Geothermal Resources, San Fransico, 2,* 1445-1449.

Thórarinsdóttir, R.I., 2000: *Corrosion of copper and copper alloys in geothermal district heating water containing sulphide, Part I.* Technical University of Denmark, unpublished Ph.D thesis, 178 pp.

Wambugu, J.M., 1996: Assessment of Olkaria-Northeast geothermal reservoir, Kenya based on well discharge chemistry. Report 20 in: *Geothermal Training in Iceland 1996.* UNU G.T.P., Iceland, 481-509.

APPENDIX I: X10 binocular descriptions for samples at trial pH 4 and 7 in condensate

Sample no.	Sample type	Sample description
pH 7 - Hot condensate fluids		
A3	Galv. mild steel	Slight grey coating, most had scratched off due to rubbing of material because of poor storage
B3	Zinc plate	Slight tarnish evident on the surfaces. Most of the sample remained intact. Slight pitting observed on the sample.
C3	Mild steel	Dark grey coating still adherent, although part has been removed. Pitting evident on the sample
D3	Aluminum	Slightly grey coating still evident, although most had scratched off.
E3	Brass	Greyish ark coating covered the sample in some parts.
F3	Copper	Black adherent coating, though most had scratched off from the surface of the coupon. Slight pits present.
pH 7 - Cold condensate fluids		
A4	Galv. mild steel	Slight grey coating. Metal sample etched due to rubbing and scratching. It is almost unchanged.
B4	Zinc plate	
C4	Mild steel	Rust-like material evident on the sample. Pitting also evident.
D4	Aluminum	Almost unchanged. Metal luster is intact. Scratches from rubbing evident
E4	Brass	Dark coating on parts of the sample. Part of it rubbed due to poor storage.
F4	Copper	Slightly dark metallic luster of copper intact. Coating rubbed off

Sample no.	Sample type	Sample description
pH 4 - Hot condensate fluids		
A9	Galv. mild steel	Slight grey coating evident but not extensive. Has rubbed off or scratched.
B9	Zinc plate	Adherent rust like material still covers the coupon though most has peeled off due to poor storage. Pitting present
C9	Mild steel	Black adherent coating evident, partly peeled off but still extensive. Pitting present.
D9	Aluminum	Slight grey coating on sample, most has peeled off. Colour of the metallic luster still remains.
E9	Brass	Black adherent coating, partly peeled off. Metallic luster exposed on some parts of the sample after peeling.
F9	Copper	Black adherent coating, appears to have peeled off on parts of the coupon.
pH 4 - Cold condensate fluids		
A10	Galv. mild steel	Patches of grey coating appear adherent, have been removed in most parts.
B10	Zinc plates	A thin grey coating exposed on some parts of the sample, most scratched and peeled off.
C10	Mild steel	Adherent rust material evident on the sample probably iron oxide, loose material scratched off.
D10	Aluminum	Surface of material remained the same, slight scratches and etches on surface.
E10	Brass	Patches of black coating that is adherent exposed on some parts of the sample. Coating has peeled off. Original metallic luster exposed.
F10	Copper	Black coating evident though most has peeled off. Original metallic luster exposed on some parts of sample

NB: This description was done a long time after the field exposure of the samples to the fluids and the samples were not well stored to preserve the original contents of the corrosion

APPENDIX II: Results of Scanning Electron Microcope

Sample C 4: Mild steel specimen in cold condensate at trial pH 7

Spectrum processing : No peaks omitted
Processing option : All elements analysed (normalised)
Number of iterations = 4

Standard :

C	$CaCO_3$	1-jún-1999 12:00 AM
O	SiO_2	1-jún-1999 12:00 AM
Mg	MgO	1-jún-1999 12:00 AM
Al	Al_2O_3	1-jún-1999 12:00 AM
S	FeS_2	1-jún-1999 12:00 AM
Mn	Mn	1-jún-1999 12:00 AM
Fe	Fe	1-jún-1999 12:00 AM

Element	App conc.	Intensity corrn.	Weight%	Weight% sigma	Atomic%
C K	5.07	0.4948	9.08	0.35	20.33
O K	43.94	1.3207	29.51	0.29	49.58
Mg K	0.11	0.4375	0.23	0.07	0.25
Al K	0.17	0.5604	0.27	0.06	0.26
S K	0.70	0.8755	0.71	0.05	0.60
Mn K	0.33	0.8926	0.32	0.08	0.16
Fe K	61.47	0.9100	59.88	0.35	28.82
Total			100.00		

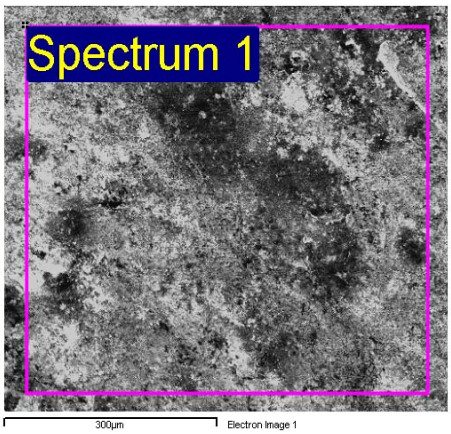

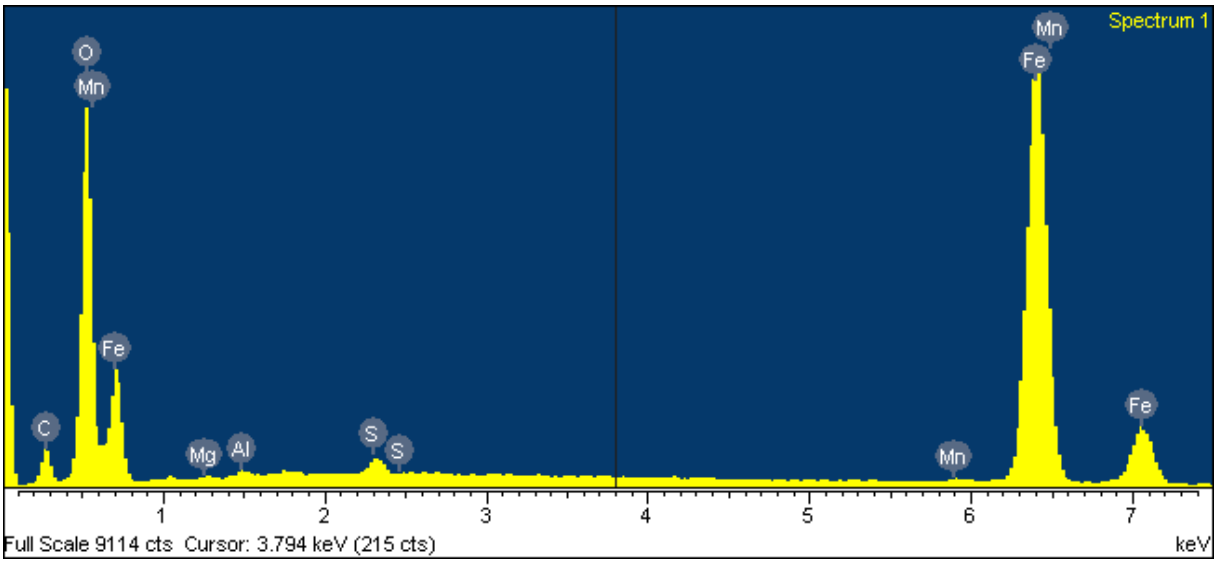

Sample C 9: Mild steel specimen in hot condensate at trial pH 4

Spectrum processing : No peaks omitted
Processing option : All elements analysed (normalised)
Number of iterations = 5

Standard :

C	$CaCO_3$	1-jún-1999 12:00 AM
O	SiO_2	1-jún-1999 12:00 AM
Al	Al_2O_3	1-jún-1999 12:00 AM
Si	SiO2	1-jún-1999 12:00 AM
S	FeS_2	1-jún-1999 12:00 AM
Fe	Fe	1-jún-1999 12:00 AM
Cu	Cu	1-jún-1999 12:00 AM
Zn	Zn	1-jún-1999 12:00 AM

Element	App conc.	Intensity corrn.	Weight%	Weight% sigma	Atomic%
C K	4.75	0.3782	13.30	0.51	28.07
O K	25.10	1.0181	26.12	0.35	41.38
Al K	0.42	0.5998	0.74	0.07	0.69
Si K	0.40	0.7204	0.59	0.06	0.54
S K	6.23	0.8897	7.42	0.13	5.86
Fe K	42.92	0.8957	50.77	0.42	23.04
Cu K	0.45	0.8114	0.58	0.14	0.23
Zn K	0.37	0.8193	0.48	0.16	0.18
Total			100		

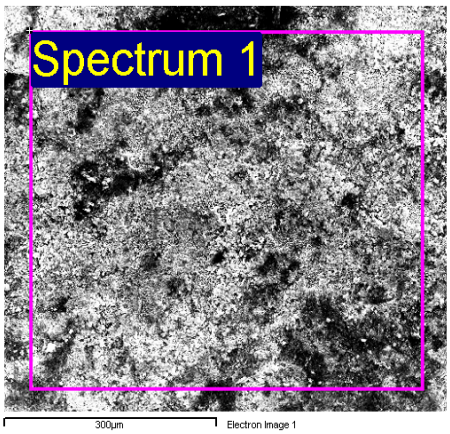

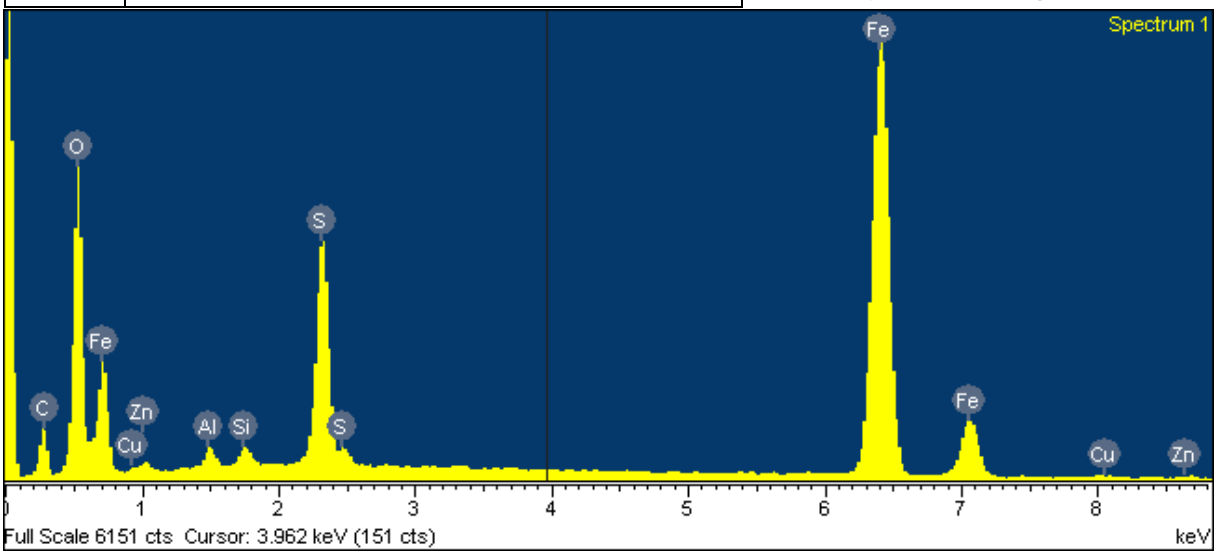

Sample C 10: Mild steel specimen in cold condensate at trial pH 4

Spectrum processing : No peaks omitted
Processing option : All elements analysed (normalised)
Number of iterations = 5

Standard :

C	$CaCO_3$	1-jún-1999 12:00 AM
O	SiO_2	1-jún-1999 12:00 AM
Mg	MgO	1-jún-1999 12:00 AM
Al	Al_2O_3	1-jún-1999 12:00 AM
S	FeS_2	1-jún-1999 12:00 AM
Mn	Mn	1-jún-1999 12:00 AM
Fe	Fe	1-jún-1999 12:00 AM

Element	App conc.	Intensity corrn.	Weight%	Weight% sigma	Atomic%
C K	7.08	0.5188	11.70	0.40	23.96
O K	49.23	1.2625	33.43	0.30	51.39
Al K	0.20	0.5786	0.29	0.05	0.27
Si K	0.41	0.7030	0.50	0.05	0.44
S K	0.35	0.8787	0.34	0.05	0.26
Cl K	0.09	0.8039	0.09	0.04	0.07
Fe K	56.04	0.8959	53.64	0.35	23.62
Total			100.00		

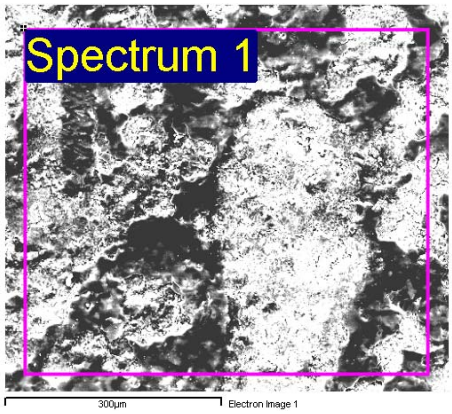

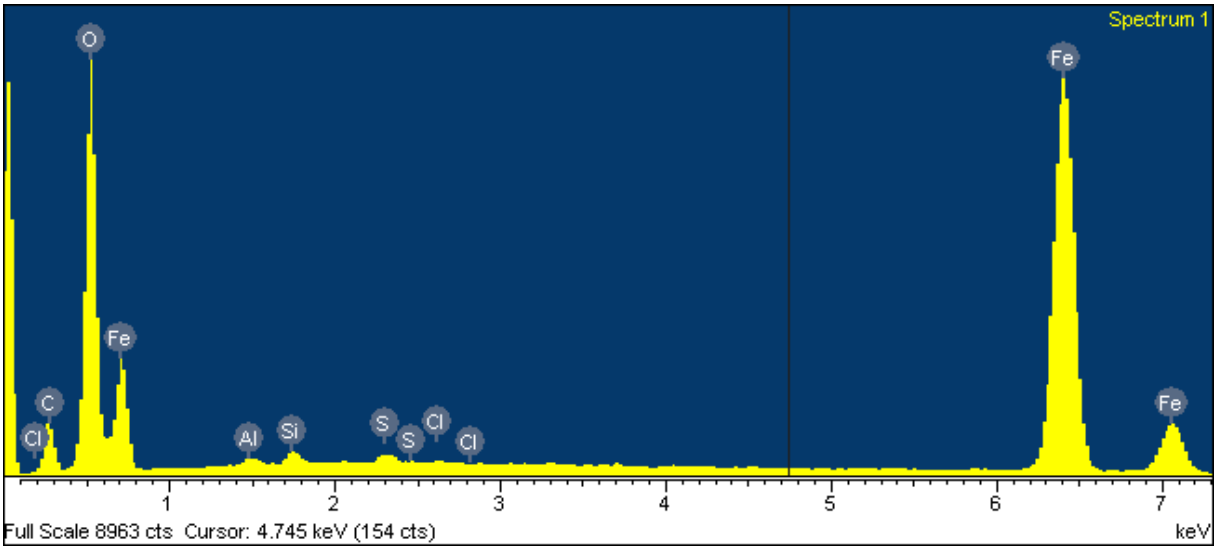

APPENDIX III: Weight loss measurements and corrosion rates calculations

Weight changes - hot condensate

							Average dimensions of coupons													
							Density				X-sectional									
pH	4	5	6	7	9		(mg/mm^3)	ID	OD	HT	area (mm^2)	ML(pH4)	ML(pH5)	ML(pH6)	ML(pH7)	ML(pH 9)	CR(pH4)	CR (pH5)	CR (pH 6)	CR (pH7)	CR9(pH9)
Galv	-0.2172	-0.055	-0.18	-0.009	-0.0058		7.85	13.5	25.25	2.9	1068.67	-25.887	-6.556	-21.480	-1.037	-0.696	-2363.80	-498.31	-2852.93	-128.04	-135.57
Mild steel	-0.2943	-0.0982	-0.1009	-0.0609	-0.0497		7.86	12.93	24.95	3.1	1084.71	-34.519	-11.521	-11.830	-7.139	-5.834	-3151.92	-875.67	-1571.18	-881.40	-1136.53
Al	0.0000	0.0166	-0.0082	-0.0165	-0.0500		2.69	12.65	25.25	2.2	1012.47	0.000	6.110	-3.026	-6.052	-18.355	0.00	464.38	-401.86	-747.18	-3575.55
Brass	-0.3151	-0.0733	-0.1106	-0.0145	-0.0291		8.75	14	22	1.2	588.34	-61.210	-14.247	-21.475	-2.818	-5.659	-5589.16	-1082.90	-2852.24	-347.98	-1102.38
Cu	-0.1355	-0.0074	-0.0419	-0.0223	-0.0248		8.94	12.25	25.25	2.5	1060.71	-14.288	-0.785	-4.416	-2.356	-2.610	-1304.66	-59.63	-586.57	-290.85	-508.47
hrs (hot)	96	115.25	66	71	45																

Weight changes - cold condensates

							Average dimensions of coupons													
							Density				X-sectional									
pH	4	5	6	7	9		(mg/mm^3)	ID	OD	HT	area (mm^2)	ML(pH4)	ML(pH5)	ML(pH6)	ML(pH7)	ML(pH 9)	CR(pH4)	CR(pH5)	CR(pH6)	CR(pH7)	CR9 (pH9)
Galv	-0.1013	-0.1338	-0.0174	-0.0231	-0.0058		7.85	13.5	25.25	2.9	1068.67	-12.081	-15.950	-2.069	-2.759	-0.689	-879.44	-1212.28	-274.77	-340.60	-134.18
Mild steel	-0.1281	-0.0494	-0.0186	-0.0311	-0.0368		7.86	12.93	24.95	3.1	1084.71	-15.028	-5.794	-2.179	-3.643	-4.314	-1093.95	-440.40	-289.43	-449.78	-840.35
Al	-0.0331	-0.0330	-0.0329	0.0000	-0.0912		2.69	12.65	25.25	2.2	1012.47	-12.136	-12.121	-12.096	0.000	-33.490	-883.44	-921.26	-1606.51	0.00	-6523.66
Brass	-0.0807	-0.1393	-0.0147	-0.0146	-0.0439		8.75	14	22	1.2	588.34	-15.673	-27.060	-2.852	-2.830	-8.533	-1140.96	-2056.76	-378.74	-349.37	-1662.29
Cu	-0.0369	-0.0619	-0.0074	-0.0148	-0.0124		8.94	12.25	25.25	2.5	1060.71	-3.895	-6.524	-0.780	-1.565	-1.306	-283.56	-495.89	-103.61	-193.27	-254.35
hrs (cold)	120. 416	115.25	66	71	45																

ML = Material loss
CR = Corrosion rate

X-Sectional area is calculated by applying the X-sectional area of a cylinder or an assumed annulus
X-sectional area of a coupon exposed (the coupons were cylindrical):

$\pi/4 * 2 * (D+ d) (D-d) + \pi * h * (D+ d)$

h = height of coupon
D = outer diameter of coupons
d = inner diameter of coupons
π = 22/6

APPENDIX IV: CHILLER calculations on fluids from RN-09

```
Calculations done for 145 DEG.C. 90 BARS
ENTHALPIES:
PURE WATER 2.6381 KCAL/MOLE
CURRENT SOLUTION 7829.8076 GAS 0 KCAL
TOTAL CURRENT ENTHALPY 7829.8076 KCAL
STARTING ENTHALPY 0 KCAL
TEMPERATURE CHANGED BY -5 DEGREES TO 140 DEGREES C.
SOLIDS AND GASES CARRIED
CHARGE BALANCE FOR SOLID MOLES = 1.654E-024
Mass of aqueous solution: 53506.421599 grams
GAS OR MIN MOLES LOG MOLES GRAMS LOG GRAMS WT PERCENT VOL(CM3)
bornite 2.372E-009 -8.625 1.19E-006 -5.924 100 2.339E-007
GAS OR MOLE FRACTION PARTIAL PRESS. FUGACITY COEF LOG FUGACITY
MINERAL OR ACTIVITY ACTIVITY COEF LOG ACTIVITY
bornite 1 1 1 0
Solid products produced: Mass: 1E-006 grams Volume: 0 CM3
Warning mineral volume may be in error because some mineral densities
were not supplied in SOLTHERM. See mineral list at top of
output.

GAS COMPOSITION AT SATURATION (2 ITERATIONS)
-----------------------------------------------------
TEMPERATURE: 140 DEG.C.
SAT. PRESSURE: 3.6769 BARS
CHARGE BALANCE FOR SOLID MOLES = -1.654E-024
Mass of aqueous solution: 53506.421599 grams
GAS OR MIN MOLES LOG MOLES GRAMS LOG GRAMS WT PERCENT VOL(CM3)
bornite 2.384E-009 -8.623 1.196E-006 -5.922 100 2.35E-007
GAS OR MOLE FRACTION PARTIAL PRESS. FUGACITY COEF LOG FUGACITY
MINERAL OR ACTIVITY ACTIVITY COEF LOG ACTIVITY
bornite 1 1 1 0
Solid products produced: Mass: 1E-006 grams Volume: 0 CM3
Warning mineral volume may be in error because some mineral densities
were not supplied in SOLTHERM. See mineral list at top of
output.
GAS COMPOSITION AT SATURATION (2 ITERATIONS)
-----------------------------------------------------
TEMPERATURE: 135 DEG.C.
SAT. PRESSURE: 3.1861 BARS
CHARGE BALANCE FOR SOLID MOLES = 0
Mass of aqueous solution: 53506.421599 grams
GAS OR MIN MOLES LOG MOLES GRAMS LOG GRAMS WT PERCENT VOL(CM3)
bornite 2.394E-009 -8.621 1.202E-006 -5.92 100 2.361E-007
GAS OR MOLE FRACTION PARTIAL PRESS. FUGACITY COEF LOG FUGACITY
MINERAL OR ACTIVITY ACTIVITY COEF LOG ACTIVITY
bornite 1 1 1 0
Solid products produced: Mass: 1E-006 grams Volume: 0 CM3
Warning mineral volume may be in error because some mineral densities
were not supplied in SOLTHERM. See mineral list at top of
output.
GAS COMPOSITION AT SATURATION (2 ITERATIONS)
-----------------------------------------------------
TEMPERATURE: 130 DEG.C.
SAT. PRESSURE: 2.7492 BARS
GAS MOLE FRAC. PHI FUGACITY PARTIAL P. (BARS)
HARGE BALANCE FOR SOLID MOLES = -3.309E-024
Mass of aqueous solution: 53506.421597 grams
GAS OR MIN MOLES LOG MOLES GRAMS LOG GRAMS WT PERCENT VOL(CM3)
bornite 2.394E-009 -8.621 1.202E-006 -5.92 52 2.361E-007
sphaleri 1.138E-008 -7.944 1.109E-006 -5.955 48 2.713E-007
GAS OR MOLE FRACTION PARTIAL PRESS. FUGACITY COEF LOG FUGACITY
MINERAL OR ACTIVITY ACTIVITY COEF LOG ACTIVITY
bornite 1 1 1 0
sphaleri 1 1 1 0
Solid products produced: Mass: 2E-006 grams Volume: 1E-006 CM3
Warning mineral volume may be in error because some mineral densities
were not supplied in SOLTHERM. See mineral list at top of
output.
GAS COMPOSITION AT SATURATION (2 ITERATIONS)
-----------------------------------------------------
TEMPERATURE: 130 DEG.C.
SAT. PRESSURE: 2.7492 BARS
CHARGE BALANCE FOR SOLID MOLES = -1.489E-023
Mass of aqueous solution: 53506.421587 grams
GAS OR MIN MOLES LOG MOLES GRAMS LOG GRAMS WT PERCENT VOL(CM3)
bornite 2.405E-009 -8.619 1.207E-006 -5.918 9.198 2.371E-007
sphaleri 1.223E-007 -6.913 1.191E-005 -4.924 90.8 2.913E-006
GAS OR MOLE FRACTION PARTIAL PRESS. FUGACITY COEF LOG FUGACITY
MINERAL OR ACTIVITY ACTIVITY COEF LOG ACTIVITY
bornite 1 1 1 0
sphaleri 1 1 1 0
Solid products produced: Mass: 1.3E-005 grams Volume: 3E-006 CM3
Warning mineral volume may be in error because some mineral densities
were not supplied in SOLTHERM. See mineral list at top of
output.
GAS COMPOSITION AT SATURATION (2 ITERATIONS)
-----------------------------------------------------
TEMPERATURE: 125 DEG.C.
SAT. PRESSURE: 2.3617 BARS
```

```
CHARGE BALANCE FOR SOLID MOLES = -3.309E-024
Mass of aqueous solution: 53506.421579 grams
GAS OR MIN MOLES LOG MOLES GRAMS LOG GRAMS WT PERCENT VOL(CM3)
bornite 2.415E-009 -8.617 1.212E-006 -5.917 5.777 2.381E-007
sphaleri 2.028E-007 -6.693 1.976E-005 -4.704 94.22 4.833E-006
GAS OR MOLE FRACTION PARTIAL PRESS. FUGACITY COEF LOG FUGACITY
MINERAL OR ACTIVITY ACTIVITY COEF LOG ACTIVITY
bornite 1 1 1 0
sphaleri 1 1 1 0
Solid products produced: Mass: 2.1E-005 grams Volume: 5E-006 CM3
Warning mineral volume may be in error because some mineral densities
were not supplied in SOLTHERM. See mineral list at top of
output.
GAS COMPOSITION AT SATURATION (2 ITERATIONS)
-----------------------------------------------------
TEMPERATURE: 120 DEG.C.
SAT. PRESSURE: 2.0195 BARS
CHARGE BALANCE FOR SOLID MOLES = -3.143E-023
Mass of aqueous solution: 53506.421579 grams
GAS OR MIN MOLES LOG MOLES GRAMS LOG GRAMS WT PERCENT VOL(CM3)
bornite 2.415E-009 -8.617 1.212E-006 -5.917 5.749 2.381E-007
sphaleri 2.028E-007 -6.693 1.976E-005 -4.704 93.76 4.833E-006
cattieri 8.35E-010 -9.078 1.027E-007 -6.988 0.4874 4.109E-008
GAS OR MOLE FRACTION PARTIAL PRESS. FUGACITY COEF LOG FUGACITY
MINERAL OR ACTIVITY ACTIVITY COEF LOG ACTIVITY
bornite 1 1 1 0
sphaleri 1 1 1 0
cattieri 1 1 1 0
Solid products produced: Mass: 2.1E-005 grams Volume: 5E-006 CM3
Warning mineral volume may be in error because some mineral densities
were not supplied in SOLTHERM. See mineral list at top of
output.
GAS COMPOSITION AT SATURATION (2 ITERATIONS)
-----------------------------------------------------
TEMPERATURE: 120 DEG.C.
SAT. PRESSURE: 2.0195 BARS
GAS MOLE FRAC. PHI FUGACITY PARTIAL P. (BARS)
CHARGE BALANCE FOR SOLID MOLES = -6.948E-023
Mass of aqueous solution: 53506.421573 grams
GAS OR MIN MOLES LOG MOLES GRAMS LOG GRAMS WT PERCENT VOL(CM3)
bornite 2.424E-009 -8.615 1.216E-006 -5.915 4.51 2.39E-007
cattieri 2.396E-009 -8.621 2.948E-007 -6.53 1.093 1.179E-007
sphaleri 2.613E-007 -6.583 2.546E-005 -4.594 94.4 6.226E-006
GAS OR MOLE FRACTION PARTIAL PRESS. FUGACITY COEF LOG FUGACITY
MINERAL OR ACTIVITY ACTIVITY COEF LOG ACTIVITY
bornite 1 1 1 0
cattieri 1 1 1 0
sphaleri 1 1 1 0
Solid products produced: Mass: 2.7E-005 grams Volume: 7E-006 CM3
Warning mineral volume may be in error because some mineral densities
were not supplied in SOLTHERM. See mineral list at top of
output.
GAS COMPOSITION AT SATURATION (2 ITERATIONS)
-----------------------------------------------------
TEMPERATURE: 115 DEG.C.
SAT. PRESSURE: 1.7186 BARS
CHARGE BALANCE FOR SOLID MOLES = 6.617E-023
Mass of aqueous solution: 53506.421572 grams
GAS OR MIN MOLES LOG MOLES GRAMS LOG GRAMS WT PERCENT VOL(CM3)
cattieri 2.395E-009 -8.621 2.947E-007 -6.531 1.053 1.179E-007
sphaleri 2.613E-007 -6.583 2.545E-005 -4.594 90.96 6.225E-006
chalcopy 1.219E-008 -7.914 2.236E-006 -5.65 7.991 5.22E-007
GAS OR MOLE FRACTION PARTIAL PRESS. FUGACITY COEF LOG FUGACITY
MINERAL OR ACTIVITY ACTIVITY COEF LOG ACTIVITY
cattieri 1 1 1 0
sphaleri 1 1 1 0
chalcopy 1 1 1 0
Solid products produced: Mass: 2.8E-005 grams Volume: 7E-006 CM3
Warning mineral volume may be in error because some mineral densities
were not supplied in SOLTHERM. See mineral list at top of
output.
GAS COMPOSITION AT SATURATION (2 ITERATIONS)
-----------------------------------------------------
TEMPERATURE: 115 DEG.C.
SAT. PRESSURE: 1.7186 BARS
CHARGE BALANCE FOR SOLID MOLES = 1.654E-024
Mass of aqueous solution: 53506.421572 grams
GAS OR MIN MOLES LOG MOLES GRAMS LOG GRAMS WT PERCENT VOL(CM3)
cattieri 2.395E-009 -8.621 2.947E-007 -6.531 1.053 1.179E-007
chalcopy 1.219E-008 -7.914 2.236E-006 -5.65 7.99 5.22E-007
sphaleri 2.613E-007 -6.583 2.545E-005 -4.594 90.95 6.225E-006
galena 1.14E-011 -10.943 2.728E-009 -8.564 0.009746 3.59E-010
GAS OR MOLE FRACTION PARTIAL PRESS. FUGACITY COEF LOG FUGACITY
MINERAL OR ACTIVITY ACTIVITY COEF LOG ACTIVITY
cattieri 1 1 1 0
chalcopy 1 1 1 0
sphaleri 1 1 1 0
galena 1 1 1 0
Solid products produced: Mass: 2.8E-005 grams Volume: 7E-006 CM3
Warning mineral volume may be in error because some mineral densities
were not supplied in SOLTHERM. See mineral list at top of
output.
```

```
GAS     COMPOSITION                 AT      SATURATION      (2 ITERATIONS)
--------------------------------------------------------
TEMPERATURE: 115  DEG.C.
SAT.    PRESSURE:   1.7186          BARS
GAS     MOLE    FRAC.               PHI     FUGACITY PARTIAL P.     (BARS)
CHARGE          BALANCE             FOR     SOLID   MOLES   =       -5.79E-024
Mass    of      aqueous             solution:       53506.421567    grams
GAS     OR      MIN MOLES           LOG     MOLES   GRAMS   LOG     GRAMS   WT      PERCENT VOL(CM3)
cattieri 3.564E-009     -8.448      4.385E-007 -6.358       1.339   1.754E-007
chalcopy 1.229E-008     -7.91       2.255E-006 -5.647       6.884   5.264E-007
galena  2.05E-009       -8.688      4.904E-007 -6.309       1.497   6.454E-008
sphaleri 3.035E-007     -6.518      2.957E-005 -4.529       90.28   7.233E-006
GAS     OR      MOLE                FRACTION PARTIAL PRESS. FUGACITY COEF   LOG     FUGACITY
MINERAL         OR  ACTIVITY        ACTIVITY COEF   LOG     ACTIVITY
cattieri 1      1   1               0
chalcopy 1      1   1               0
galena  1       1   1               0
sphaleri 1      1   1               0
Solid   products    produced:       Mass:   3.3E-005    grams   Volume:     8E-006  CM3
Warning mineral     volume          may     be      in      error   because some    mineral densities
were    not         supplied        in      SOLTHERM.       See     mineral list    at      top     of
        output.
GAS     COMPOSITION                 AT      SATURATION      (2 ITERATIONS)
--------------------------------------------------------
TEMPERATURE: 110  DEG.C.
SAT.    PRESSURE:   1.4553          BARS
CHARGE          BALANCE             FOR     SOLID   MOLES   =       -6.948E-023
Mass    of      aqueous             solution:       53506.421564    grams
GAS     OR      MIN MOLES           LOG     MOLES   GRAMS   LOG     GRAMS   WT      PERCENT VOL(CM3)
cattieri 4.433E-009     -8.353      5.455E-007 -6.263       1.507   2.182E-007
chalcopy 1.237E-008     -7.908      2.271E-006 -5.644       6.273   5.3E-007
galena  3.484E-009      -8.458      8.335E-007 -6.079       2.303   1.097E-007
sphaleri 3.34E-007      -6.476      3.255E-005 -4.487       89.92   7.96E-006
GAS     OR      MOLE                FRACTION PARTIAL PRESS. FUGACITY COEF   LOG     FUGACITY
MINERAL         OR  ACTIVITY        ACTIVITY COEF   LOG     ACTIVITY
cattieri 1      1   1               0
chalcopy 1      1   1               0
galena  1       1   1               0
sphaleri 1      1   1               0
Solid   products    produced:       Mass:   3.6E-005    grams   Volume:     9E-006  CM3
Warning mineral     volume          may     be      in      error   because some    mineral densities
were    not         supplied        in      SOLTHERM.       See     mineral list    at      top     of
        output.
GAS     COMPOSITION                 AT      SATURATION      (2 ITERATIONS)
--------------------------------------------------------
TEMPERATURE: 105  DEG.C.
CHARGE          BALANCE             FOR     SOLID   MOLES   =       -2.151E-022
Mass    of      aqueous             solution:       53506.421392    grams
GAS     OR      MIN MOLES           LOG     MOLES   GRAMS   LOG     GRAMS   WT      PERCENT VOL(CM3)
cattieri 4.354E-009     -8.361      5.358E-007 -6.271       0.2577  2.143E-007
chalcopy 1.231E-008     -7.91       2.258E-006 -5.646       1.086   5.271E-007
galena  3.424E-009      -8.465      8.192E-007 -6.087       0.394   1.078E-007
sphaleri 3.323E-007     -6.478      3.238E-005 -4.49        15.57   7.918E-006
pyrite  1.433E-006      -5.844      0.0001719  -3.765       82.69   3.431E-005
GAS     OR      MOLE                FRACTION PARTIAL PRESS. FUGACITY COEF   LOG     FUGACITY
MINERAL         OR  ACTIVITY        ACTIVITY COEF   LOG     ACTIVITY
cattieri 1      1   1               0
chalcopy 1      1   1               0
galena  1       1   1               0
sphaleri 1      1   1               0
pyrite  1       1   1               0
Solid   products    produced:       Mass:   0.000208    grams   Volume:     4.3E-005    CM3
Warning mineral     volume          may     be      in      error   because some    mineral densities
were    not         supplied        in      SOLTHERM.       See     mineral list    at      top     of
        output.
GAS     COMPOSITION                 AT      SATURATION      (2 ITERATIONS)
--------------------------------------------------------
TEMPERATURE: 105  DEG.C.
CHARGE          BALANCE             FOR     SOLID   MOLES   =       -5.84E-022
Mass    of      aqueous             solution:       53506.421167    grams
GAS     OR      MIN MOLES           LOG     MOLES   GRAMS   LOG     GRAMS   WT      PERCENT VOL(CM3)
cattieri 4.94E-009      -8.306      6.078E-007 -6.216       0.1405  2.431E-007
chalcopy 1.228E-008     -7.911      2.253E-006 -5.647       0.5207  5.26E-007
galena  4.392E-009      -8.357      1.051E-006 -5.978       0.2428  1.383E-007
pyrite  3.288E-006      -5.483      0.0003945  -3.404       91.15   7.87E-005
sphaleri 3.529E-007     -6.452      3.438E-005 -4.464       7.945   8.409E-006
GAS     OR      MOLE                FRACTION PARTIAL PRESS. FUGACITY COEF   LOG     FUGACITY
MINERAL         OR  ACTIVITY        ACTIVITY COEF   LOG     ACTIVITY
cattieri 1      1   1               0
chalcopy 1      1   1               0
galena  1       1   1               0
pyrite  1       1   1               0
sphaleri 1      1   1               0
Solid   products    produced:       Mass:   0.000433    grams   Volume:     8.8E-005    CM3
Warning mineral     volume          may     be      in      error   because some    mineral densities
were    not         supplied        in      SOLTHERM.       See     mineral list    at      top     of
        output.
GAS     COMPOSITION                 AT      SATURATION      (2 ITERATIONS)
--------------------------------------------------------
TEMPERATURE: 100  DEG.C.    SAT.    PRESSURE:       1.027   BARS
```